OPTIMAL CLOSURES IN HYDRODYNAMIC MODELS

OPTIMAL CLOSURES IN HYDRODYNAMIC MODELS

BY

PRITPAL MATHARU, B.Sc.

A Thesis Submitted to the School of Graduate Studies

in Partial Fulfilment of the Requirements

for the Degree of Masters of Science

Masters of Science (2018) McMaster University
Department of Mathematics and Statistics Hamilton, Ontario, Canada

TITLE: Optimal Closures in Hydrodynamic Models

AUTHOR: Pritpal Matharu
B.Sc., Applied Mathematics and Physics (The University of Western Ontario)

SUPERVISOR: Bartosz Protas

NUMBER OF PAGES: xiv, 83

Abstract

In this work, we investigate the performance limitations characterizing certain common closure models for nonlinear models of fluid flow. The need for closures arises when for computational reasons first-principles models, such as the Navier-Stokes equations, are replaced with their simplified (filtered) versions such as the Large-Eddy Simulation (LES). In the present work, we focus on a simple model problem based on the 1D Kuramoto-Sivashinsky equation with a Smagorinsky-type eddy-viscosity closure model. The eddy viscosity is assumed to be a function of the state (flow) variable whose optimal functional form is determined in a very general form in the continuous setting. It is found by solving a PDE-constrained optimization problem in which the least-squares error between the output of the LES and the true flow evolution is minimized with respect to the functional form of the eddy viscosity. This problem is solved using a gradient-based technique utilizing a suitable adjoint-based variational data-assimilation approach implemented in the optimize-then-discretize setting using state-of-the-art techniques. The numerical computations are thoroughly validated. The obtained results indicate how the standard

Smagorinsky closure model can be refined such that the corresponding LES evolution approximates more accurately the evolution of the original (unfiltered) flow.

Acknowledgements

First and foremost, I would like to thank my supervisor Dr. Bartosz Protas, for all his guidance and advice for this research, especially during this thesis writing process. His knowledge, patience, and support have truly helped me grow professionally as a researcher and also personally. I would like to thank Dr. Nicholas Kevlahan and Dr. Stephen Tullis, for their review, input, and helpful recommendations for this thesis. In addition, I would like to acknowledge and thank the members of the Mathematics and Statistics department at McMaster University, for providing a wonderful work environment and great conversation. I would also like to thank my fellow graduate students, for their constant encouragement and discussions in all fields of mathematics. Lastly, I am very grateful for my family and friends for their continuous support.

Contents

List of Figures

Chapter 1

Introduction and Problem Statement

1.1 Motivation

Turbulent flows occur in various fields, and are an imperative and complex topic in fluid dynamics. Understanding the complex movement of fluids is vital for various research areas, ranging from biological modelling to engineering design models for understanding fluid flows around objects such as cars and airplanes. The Navier-Stokes equations are at the centre of this field and are essential for understanding fluid flows. These equations can simply be derived from basic principles of conservation of mass and momentum of Newtonian fluids. The Navier-Stokes equation for a steady

(on-average) flow can be written as [9]

$$\begin{cases} \rho \frac{\partial v_i}{\partial t} + \rho(\boldsymbol{v} \cdot \nabla) v_i = -\frac{\partial p}{\partial x_i} + \frac{\partial \tau_{ij}}{\partial x_j}, \qquad i, j = 1, 2, 3, \\ \frac{\partial v_i}{\partial x_i} = 0, \end{cases} \tag{1.1}$$

where $\boldsymbol{v} = [v_1, v_2, v_3]^T$ is the velocity field of the fluid, p is the fluid pressure, and ρ is the density of the fluid. In equation (1.1), Einstein's convention of summation is implied by repeated indices used. The viscous stresses τ_{ij} are represented by

$$\tau_{ij} = 2\rho\nu_N S_{ij} = \rho\nu_N \left[\frac{\partial u_i}{\partial x_j} + \frac{\partial u_j}{\partial x_i} \right], \tag{1.2}$$

where ν_N is the viscosity and S_{ij} is the strain-rate tensor. The Navier-Stokes equations have been used for over a century and are one of most influential partial differential equations (PDE) in physics [7]. Although turbulent flows are extremely complicated, these straightforward equations are able to encapsulate all scales of the fluid flows. To date however, the Navier-Stokes equations remain part of the unsolved Millennium Problems [11]. Due to the complexities of solving the Navier-Stokes equations (along with other sets of equations that describe turbulent flows), we search for a computationally efficient and mathematically accurate method to obtain numerical solutions.

In fluid dynamics, a turbulent flow is typically described by eddies which contain information about the flow. Assuming the turbulent flow is homogeneous with respect to the spatial domain, it is often useful to describe the flow using Fourier space, describing the flow in terms of spatial frequency (wavenumbers) instead. A certain

eddy size is associated with a particular wavenumber, letting us observe a turbulent flow in terms of a spectrum [25]. Large eddies are considered to be the scales which dictate the main dynamics of the flow, and correspond to the low wavenumbers. The high wavenumbers, correspond to the small eddies which contain information about the smaller scales of the system. By considering turbulent flows in Fourier space, it is often viewed that energy is introduced into the system at the large scales which are considered as the energy containing eddies. Energy is then cascaded down from the large scales to the small scales, where the small scales dissipate the energy in the system [12]. These smaller scales of the system, also known as viscous eddies, do not on average transfer energy up to larger scales, indicating that there are several intermediate eddies which pass energy to the smaller dissipative eddies, which is known as the inertial subrange. Typically for turbulent flows, there are only a few energy containing scales, and the remaining spectrum transfers energy to the dissipative scales.

A direct numerical simulation (DNS) is a "brute-force" method used to numerically compute turbulent flows, which involves a wide range of spatial scales, providing an accurate way to simulate the flows down to the smallest dissipative scale (typically denoted as the Kolmogorov scale) [9]. As a result of computing down to the Kolmogorov scale, this method is extremely computationally expensive, even with the advancement of modern super computers. In DNS, majority of computations are spent computing the small dissipative scales. Subsequently, large eddy simulations (LES) were developed as a computationally efficient viable substitute. LES models

rely on large scales of turbulent flows containing the majority of the energy and information, which are cascaded down to the smaller scales (but again we emphasize the smaller scales do not on average transfer energy up to the large scales). Consequently, in LES models, large eddies are computed exactly without the presence of the small scales. This can be considered as an averaging process, where the mean velocity is separated from the turbulent fluctuations. Performing time-averaging, denoted by $\bar{\cdot}$ (bar), to the Navier-Stokes, we obtain [9]

$$\rho(\overline{\boldsymbol{v}} \cdot \nabla)\overline{v}_i = -\frac{\partial \overline{p}}{\partial x_i} + \frac{\partial}{\partial x_j}\left[\, \overline{\tau}_{ij} - \rho\overline{v_i' v_j'} \,\right],$$

where $\rho\overline{v_i' v_j'}$ can be interpreted as an additional "force" due to turbulent fluctuations. This term is known as the Reynolds stresses $\tau_{ij}^R = -\rho\overline{v_i' v_j'}$, which acts like an additional stress term induced from the turbulent fluctuations. This result is the time-averaged equation

$$\rho(\overline{\boldsymbol{v}} \cdot \nabla)\overline{v}_i = -\frac{\partial \overline{p}}{\partial x_i} + \frac{\partial}{\partial x_j}\left[\, \overline{\tau}_{ij} + \tau_{ij}^R \,\right], \tag{1.3}$$

When given a sufficient number of boundary conditions along with the equation in (1.1) to formulate a well-determined system, (1.3) introduces an additional unknown. The introduction of the Reynolds stresses causes the system to have more unknowns than equations, known as the "closure problem". This problem consists of expressing the Reynold stresses, defined in terms of quantities which are not computed ($\boldsymbol{v}'$) in terms of quantities which are computed ($\overline{\boldsymbol{v}}$). The nonlinear nature of the equations used to describe fluid flows, along with this filtering (averaging) process results in a

sub-grid parameterization where interactions between the small and the large scales need to be modelled.

1.2 Smagorinsky Model

Due to the nonlinear terms in the Navier-Stokes equations, this closure problem arises when filtering or statistically averaging, such that there are more unknowns than there are equations. Closure models are a common method to resolve this issue. The Smagorinsky model [23] and many of its modifications have been widely used as a closure model to compute LES, which include use in the context of formulating reduced-order models for Navier-Stokes [20] as well as applying this to other turbulent equations [17]. The Smagorinsky model is known as being an eddy viscosity type closure model, assumes the eddy viscosity is dependent upon the rate of the strain tensor computed for the averaged field. The filtered version of the Navier-Stokes equation can be written with an eddy viscosity closure as

$$\frac{\partial \overline{v}_i}{\partial t} + \frac{\partial}{\partial x_j}(\,\overline{v}_i \overline{v}_j\,) = -\frac{1}{\rho}\frac{\partial \overline{p}}{\partial x_i} + 2\frac{\partial}{\partial x_j}\left[(\nu_N + \nu_R)\,\overline{S}_{ij}\right], \qquad i,j = 1,2,3, \tag{1.4}$$

where using a Smagorinsky model would prescribe the eddy viscosity ν_R as [9], [18]

$$\nu_R = C_s^2 L^2 \left(2\overline{S}_{ij}\overline{S}_{ij}\right)^{1/2}. \tag{1.5}$$

The eddy viscosity is also comprised of the filter width L, and an adjustable parameter C_s called the Smagorinsky coefficient. This eddy viscosity is dependent on the resolved velocity field, in particular the velocity gradients, but is intended to characterize the unresolved subgrid scales. Although this model is rather simple, it is extremely popular and is used as the basis of several more advanced models. It should be noted that the eddy viscosity is artificially introduced, and is added to the viscosity from the initial set of equations. In the original formulation the Smagorinsky coefficient was taken as a constant, but methods have been introduced to dynamically compute this coefficient based on the resolved scales (known as Germano models), with the preferred form proposed by Lilly [16]. The Smagorinsky model also has major flaws, which include being too dissipative near walls [9]. Another major drawback of the Smagorinsky model is that it assumes the eddy viscosity is zero if and only if the velocity gradient is zero and the eddy viscosity is positive elsewhere, implying the closure term will be strictly dissipative [21]. Although the Smagorinsky model is extremely popular, the problems of its calibration and validation have been traditionally dominated by empiricism, and the goal of this thesis is to introduce a degree of mathematical rigour to this field. More precisely, we will develop an optimization-based approach that will allow one to assess the fundamental possibilities and performance limitations inherent in this class of closure models. By relying on rigorous methods of mathematical optimization, this research will provide a systematic and objective assessment of the fundamental opportunities and limitations inherent in the Smagorinsky model. As such, it will therefore offer guidance to the LES community in their development of closure models.

1.3 Kuramoto-Sivashinsky Equation

Due to the complexity and high computational expense of the Navier-Stokes equations, we shall consider a one-dimensional model. The simple system we shall consider is the Kuramoto-Sivashinsky equation with periodic boundary conditions

$$\begin{cases} \frac{\partial w(t,x)}{\partial t} + \nu_1 \frac{\partial^4 w(t,x)}{\partial x^4} + \nu_2 \left[\frac{\partial^2 w(t,x)}{\partial x^2} + w(t,x) \frac{\partial w(t,x)}{\partial x} \right] = 0, & (t,x) \in [0,T] \times \Omega, \\ \frac{\partial^{(i)} w}{\partial x^{(i)}}(t,0) = \frac{\partial^{(i)} w}{\partial x^{(i)}}(t,2\pi), & i = 0,\ldots,3, \\ w(0,x) = w_0(x), \end{cases} \tag{1.6}$$

where $\Omega = (0, 2\pi)$, $T > 0$ is some time for which the system is solved over, $\nu_1, \nu_2 \in \mathbb{R}^+$ are constants, and $w_0(x)$ is an appropriate initial condition for the system.

Originally this equation was proposed as a model for instabilities on interfaces and flame fronts [22], and "phase turbulence" in chemical reactions [15]. However, in this investigation we are not concerned with the application of these equations or what they model, and more interested in the dynamics of the equation and its turbulent/ chaotic behaviour as a "one-dimensional" turbulent system. More importantly, Kuramoto-Sivashinsky equation shares some general features with the Navier-Stokes equations. In particular, the second-order derivative term which is a destabilizing energy source, responsible for unstable large scales. Solutions to the Kuramoto-Sivashinsky equation sustain their behaviour due to this negative diffusion term. The fourth-order derivative is a stabilizing energy sink, dissipating energy at the

small scales. Lastly, the nonlinear term responsible for the turbulent behaviour, transferring energy from large scales to small scales. Although it may be difficult to exactly define what "turbulent behaviour" is [9], it is often agreed upon that a turbulent flow has multiscale features, chaotic behaviour, and/ or is spatio-temporally complex. Kuramoto-Sivashinsky contains all these features, and the constants ν_1, ν_2 can be used to control the turbulent behaviour (which shall be further discussed in Chapter 3). A schematic of a typical spectrum of Kuramoto-Sivashinsky is given in Figure 1.1, where the ranges in which the energy is introduced into the system (large eddies), energy is cascaded from large to small scales (inertial subrange), and energy is dissipated (small eddies) are indicated. Typically viscous Burgers equation [4] is considered as the one dimensional analogous version Navier-Stokes, but Burgers equation is simply the heat equation "in disguise" by using the Cole-Hopf transformation [5], [13]. The high order derivatives in Kuramoto-Sivashinsky also adds additional mathematical and numerical complexity, which makes it a more interesting problem to investigate.

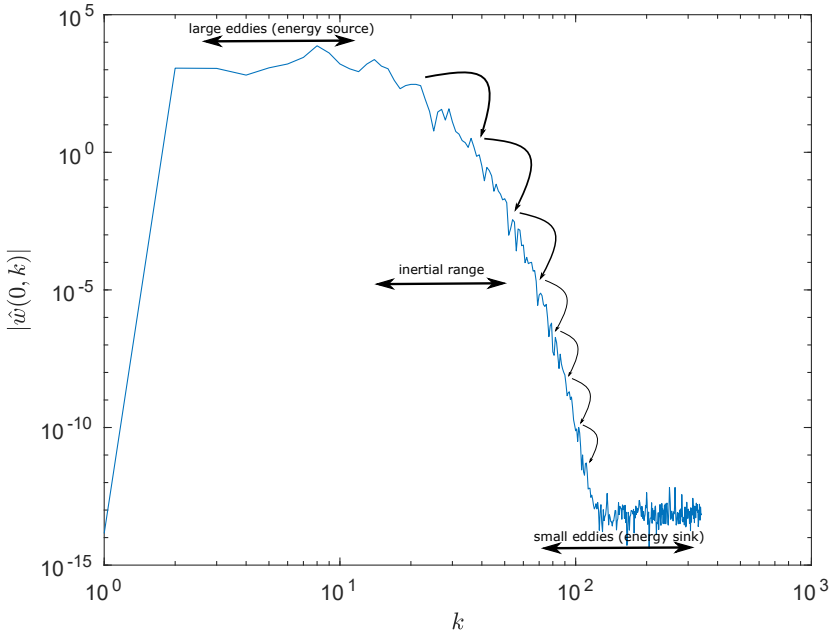

Figure 1.1: A schematic of a typical Fourier spectrum of a solution of the Kuramoto-Sivashinsky, representing the energy cascade from large scales to smaller scales (since eddies are difficult to visualize in one-dimension, we use Fourier modes). The description of numerical methods and parameters to generate this plot are given below in Chapters 3, 4, and 5.

1.4 Main Contributions and Outline of Thesis

In this thesis, we focus upon determining the optimal form of the closure term, in particular finding the optimal eddy viscosity, for an LES system. The main contributions of this work are

- development and validation of a general optimization-based approach to determination of optimal closures in hydrodynamic models,
- insights about the "best" closure form and its fundamental performance limitations, and

- determine whether or not the Smagorinsky hypothesis is valid to be used for LES models.

The structure of this thesis is as follows: in Chapter 2 we construct an LES model for the Kuramoto-Sivashinsky equation using the Smagorinsky hypothesis. We then formulate the optimization-based approach for determining the optimal eddy viscosity. Chapter 3 describes the physical parameters used in the current investigation and the operators we shall use to observe the solutions. Chapter 4 is devoted for describing the numerical approach used to numerically discretize and address the optimization problem, in a computationally efficient and accurate method. In Chapter 5, we describe the diagnostic quantities used to compare solutions and key results of this work. In Chapter 6 we discuss the results obtained. We conclude with a summary of the thesis and a discussion of future research directions in Chapter 7.

Chapter 2

Optimal Closures

In this Chapter, we formulate an LES system for the Kuramoto-Sivashinsky equation where the closure uses a Smagorinsky-type eddy viscosity model. In order to determine the optimal form of the eddy viscosity, we formulate this as an optimization problem. This optimization procedure is formulated in a very general (continuous) setting, and a gradient used to determine the optimal eddy viscosity is derived. Finally, we ensure the gradient to be used is sufficiently smooth, such that the eddy viscosity will also remain sufficiently smooth.

2.1 LES for Kuramoto-Sivashinsky Equation

To determine an optimal closure for (1.6), we must first define the filtering operation for which scales are to be resolved and the scales to be truncated. We shall use a simple box filter, as was used in [8]. That is, for some function f, we denote the

filtered function as $\tilde{f}$, defined by

$$\widetilde{f}(x) = \int_{-\infty}^{\infty} G(x-\xi) f(\xi)\, d\xi, \tag{2.1}$$

where G is a filter kernel. The expression in (2.1) can be simplified by considering the filtering process in Fourier space. Denoting $\hat{f}$ and $\hat{G}$ to be the Fourier transforms of f and G, respectively, the convolution in (2.1) simplifies to a product in Fourier space

$$\hat{\widetilde{f}}(k) = \widehat{G}(k)\, \hat{f}(k).$$

Choosing the filter kernel G as a sharp Fourier cutoff filter (box filter), we obtain the low-pass filter

$$\widehat{G}(k) = \begin{cases} 1, & |k| \leq k_{\max}, \\ 0, & \text{otherwise}, \end{cases} \tag{2.2}$$

where $k_{\max}$ is the maximum resolved wavenumber to be computed. This filtering is applied to (1.6), to derive the filtered version of the Kuramoto-Sivashinsky equation

$$\frac{\partial \widetilde{w}}{\partial t} + \nu_1 \frac{\partial^4 \widetilde{w}}{\partial x^4} + \nu_2 \Big[\frac{\partial^2 \widetilde{w}}{\partial x^2} + \frac{1}{2} \frac{\partial \widetilde{ww}}{\partial x} \Big] = 0.$$

Since the above equation is dependent upon w, which is unknown in the LES system, we shall add a nonlinear term that is dependent on the filtered field $\widetilde{w}$. Adding this

nonlinear term to both sides of the equation

$$\frac{\partial \widetilde{w}}{\partial t} + \nu_1 \frac{\partial^4 \widetilde{w}}{\partial x^4} + \nu_2 \Big[\frac{\partial^2 \widetilde{w}}{\partial x^2} + \frac{1}{2}\frac{\partial \widetilde{ww}}{\partial x} + \frac{1}{2}\frac{\partial \widetilde{\widetilde{w}\widetilde{w}}}{\partial x}\Big] = \frac{\nu_2}{2}\frac{\partial \widetilde{\widetilde{w}\widetilde{w}}}{\partial x},$$

we can write the left side of the equation strictly in terms of the filtered field $\widetilde{w}$

$$\frac{\partial \widetilde{w}}{\partial t} + \nu_1 \frac{\partial^4 \widetilde{w}}{\partial x^4} + \nu_2 \Big[\frac{\partial^2 \widetilde{w}}{\partial x^2} + \frac{1}{2}\frac{\partial \widetilde{\widetilde{w}\widetilde{w}}}{\partial x}\Big] = \frac{\nu_2}{2}\Big[\frac{\partial \widetilde{\widetilde{w}\widetilde{w}}}{\partial x} - \frac{\partial \widetilde{ww}}{\partial x}\Big].$$

Thus, the filtered equation can be represented as,

$$\frac{\partial \widetilde{w}}{\partial t} + \nu_1 \frac{\partial^4 \widetilde{w}}{\partial x^4} + \nu_2 \Big[\frac{\partial^2 \widetilde{w}}{\partial x^2} + \frac{1}{2}\frac{\partial (\widetilde{\widetilde{w}\widetilde{w}})}{\partial x}\Big] = -M(w), \tag{2.3}$$

where $M(w)$ is the term that compensates for the absence of the small scales. The term represents the "subgrid stresses", τ, with the relation

$$\begin{aligned} M(w) =& \frac{\partial \tau}{\partial x}, \\ \tau :=& \frac{\nu_2}{2}\Big[\widetilde{ww} - \widetilde{\widetilde{w}\widetilde{w}}\Big]. \end{aligned} \tag{2.4}$$

We shall emphasize that $M(w)$ is dependent on quantities (w) which are unavailable in the LES system of the Kuramoto-Sivashinsky equation, thus $M(w)$ must be modelled as a function of strictly $\widetilde{w}$. We shall be focused upon constructing an optimal model term, in order to approximate the solution of the unfiltered solution of Kuramoto-Sivashinsky, satisfying the expression given in (1.6).

In order to determine the optimal closure form, we shall choose a typical closure hypothesis. In particular, we will use the Smagorinsky model as an ansatz to determine the optimal closure term which relies upon an eddy viscosity term [9]. In this investigation, the problem that we shall be concerned about is determining an optimal eddy viscosity such that the solutions of the filtered LES match the "exact" (DNS) solution. This procedure will also act as a validation of Smagorinsky's hypothesis for LES closure models, i.e. we address the questions: with the Smagorinsky hypothesis, in principle how well can a LES reconstruct a flow? What is the "best" LES that can be constructed, using a Smagorinsky closure model?

Regarding the construction of the model term, the Smagorinsky model relies on the energy of eddies, so this causes the eddy viscosity to be dependent on the gradient of the state variable (velocity field) which forms an additional nonlinearity. To form an appropriate Smagorinsky-type eddy viscosity, we shall formulate the eddy viscosity, ν_e, in a general framework such that

$$\nu_e := \nu_e\Big(\Big(\frac{\partial \widetilde{w}}{\partial x}\Big)^2\Big). \tag{2.5}$$

Here we use a dependence on the gradient of the velocity field squared, which is similar to the dependence of the eddy viscosity on strain-rate tensor for the Smagorinsky model for the Navier-Stokes equation. We also use the square of the velocity gradient field to ensure the eddy viscosity is remains continuous. To construct the closure and validate the Smagorinsky model, we wish to investigate the following inverse problem: Given time-dependent measurements $\{m_i(t)\}_{i=1}^N$ of the unfiltered Kuramoto-Sivashinsky flow (i.e. DNS of (1.6)), at certain points in space $\{x_i\}_{i=1}^N$,

within a time-window $t \in [0, T]$, we wish to determine an optimal eddy viscosity with the form given in (2.5), such that the solutions to the LES (given in (2.8)) best fit the measurements from the unfiltered flow.

Using the eddy viscosity relation in (2.5), we can then use the eddy viscosity to estimate the subgrid stresses (2.4)

$$\tau \approx \widetilde{\tau} = \nu_e\Big(\Big(\frac{\partial \widetilde{w}}{\partial x}\Big)^2\Big)\,\frac{\partial^3 \widetilde{w}}{\partial x^3}, \tag{2.6}$$

giving us the closure for the term M, cf. (2.4)

$$M(w) \approx \widetilde{M} = \frac{\partial}{\partial x}\Big[\nu_e\Big(\Big(\frac{\partial \widetilde{w}}{\partial x}\Big)^2\Big)\,\frac{\partial^3 \widetilde{w}}{\partial x^3}\Big]. \tag{2.7}$$

For the Kuramoto-Sivashinsky equation, we know the fourth-order term is dissipative. So, for the system given in (1.6) the energy is dissipated at the smaller scales, which are no longer resolved in the filtered equation. As a result, the closure term must act as an additional dissipation term, maintaining the same dissipation rate as in the unfiltered Kuramoto-Sivashinsky equation. Thus, this is the reason we use the particular form for the model term, given in (2.7).

Using the model closure term (2.7), we obtain the following LES system

$$\begin{aligned}
&\frac{\partial \widetilde{w}}{\partial t} + \nu_1 \frac{\partial^4 \widetilde{w}}{\partial x^4} + \nu_2\Big[\frac{\partial^2 \widetilde{w}}{\partial x^2} + \frac{1}{2}\frac{\partial(\widetilde{w}\widetilde{w})}{\partial x}\Big] = -\frac{\partial}{\partial x}\Big[\nu_e\Big(\Big(\frac{\partial \widetilde{w}}{\partial x}\Big)^2\Big)\,\frac{\partial^3 \widetilde{w}}{\partial x^3}\Big],\\
&\frac{\partial^{(i)} \widetilde{w}}{\partial x^{(i)}}(t,0) = \frac{\partial^{(i)} \widetilde{w}}{\partial x^{(i)}}(t,2\pi), \qquad i = 0,\ldots,3,\\
&\widetilde{w}(0,x) = \widetilde{w}_0(x).
\end{aligned} \tag{2.8}$$

Now, we must define and note

- $[\alpha, \beta] := \left[\min\left(\left(\frac{\partial \widetilde{w}}{\partial x} \right)^2 \right), \max\left(\left(\frac{\partial \widetilde{w}}{\partial x} \right)^2 \right) \right]$ which gives a range spanned by the square of the velocity gradient field of (2.8). We shall denote $\mathcal{I} := [\alpha, \beta]$ as the "identifiability interval",

- $\mathcal{L} := [a, b]$, where $a < \alpha$ and $b > \beta$; this is the entire domain on which we are required to determine the eddy viscosity; we note that the interval $\mathcal{L}$ contains values which are generally outside of $\mathcal{I}$ (hence, $\mathcal{I} \subset \mathcal{L}$ and $\mathcal{L} \setminus \mathcal{I} \neq \varnothing$).

Since we are dealing with real valued-solutions and we are considering the square of the velocity gradient field, a natural minimum value is to set $a = 0$.

2.2 Optimization Approach to finding Eddy Viscosity

For our eddy viscosity ν_e, we must assume some smoothness properties

$$\nu_e\Big(\Big(\frac{\partial \widetilde{w}}{\partial x} \Big)^2 \Big) \text{ piecewise } \mathrm{C}^3 \text{ on } \mathcal{L}.$$

Thus, the derivatives

$$\frac{d^{(i)}\big(\nu_e\big(\big(\frac{\partial \widetilde{w}}{\partial x}\big)^2\big)\big)}{d(\big(\frac{\partial \widetilde{w}}{\partial x}\big)^2)^{(i)}}, \qquad i = 0, \ldots, 3, \tag{2.9}$$

are at least piecewise continuous on $\mathcal{L}$. Since the eddy viscosity is dependent on the velocity gradient field squared, we shall now show ν_e is then also continuous with

respect to x. We require this property to make the optimization approach introduced below well defined. To begin, we shall note that the Kuramoto-Sivashinsky equation gives smooth unique solutions which are continuously dependent on the initial condition $w_0(x)$ [24]. Now, determining the continuity of the partial derivative of ν_e, with respect to x

$$\frac{\partial\big(\nu_e\big(\big(\frac{\partial\widetilde{w}}{\partial x}\big)^2\big)\big)}{\partial x} = 2\frac{d\big(\nu_e\big(\big(\frac{\partial\widetilde{w}}{\partial x}\big)^2\big)\big)}{d\big(\big(\frac{\partial\widetilde{w}}{\partial x}\big)^2\big)}\,\frac{\partial^2\widetilde{w}}{\partial x^2}\,\frac{\partial\widetilde{w}}{\partial x}.$$

Since we begin with an appropriate initial condition $w_0(x)$ (given in (1.6)), this shall give us piecewise continuous first and second derivatives (with respect to x) of the solution of (2.8). Thus, using (2.9) and that the x-derivatives of the solution are also continuous, we shall conclude that the derivative of ν_e with respect to x is continuous. Similarly,

$$\begin{aligned}\frac{\partial^2\big(\nu_e\big(\big(\frac{\partial\widetilde{w}}{\partial x}\big)^2\big)\big)}{\partial x^2} &= 2\,\frac{d^2\big(\nu_e\big(\big(\frac{\partial\widetilde{w}}{\partial x}\big)^2\big)\big)}{d\big(\big(\frac{\partial\widetilde{w}}{\partial x}\big)^2\big)^2}\,\frac{\partial\widetilde{w}}{\partial x}\,\frac{\partial^2\widetilde{w}}{\partial x^2}+\\ &\qquad 2\,\frac{d\big(\nu_e\big(\big(\frac{\partial\widetilde{w}}{\partial x}\big)^2\big)\big)}{d\big(\big(\frac{\partial\widetilde{w}}{\partial x}\big)^2\big)}\,\left[\Big(\frac{\partial^2\widetilde{w}}{\partial x^2}\Big)^2+\frac{\partial\widetilde{w}}{\partial x}\,\frac{\partial^3\widetilde{w}}{\partial x^3}\right].\end{aligned}$$

Again, from (2.9) along with the first, second, and third derivatives (with respect to x) of the solutions to (2.8) being piecewise continuous, then the second derivative of ν_e with respect to x is also continuous. Using similar arguments as above, we can conclude

$$\frac{\partial^{(i)}\big(\nu_e\big(\big(\frac{\partial\widetilde{w}}{\partial x}\big)^2\big)\big)}{\partial x^{(i)}}, \qquad i=0,\ldots,3, \tag{2.10}$$

are all piecewise continuous on Ω. As a result, we retain the properties of the periodic boundary conditions

$$\frac{\partial^{(i)}}{\partial x^{(i)}}\left(\nu_e\Big(\Big(\frac{\partial \widetilde{w}}{\partial x}\Big)^2\Big)\right)\Big|_{x=0} = \frac{\partial^{(i)}}{\partial x^{(i)}}\left(\nu_e\Big(\Big(\frac{\partial \widetilde{w}}{\partial x}\Big)^2\Big)\right)\Big|_{x=2\pi}, \qquad i = 0, \ldots, 3. \tag{2.11}$$

We wish to find the optimal eddy viscosity, for a given flow with the measurements $\{m_i(t)\}_{i=1}^N$. In order to determine the optimal model term, we shall reformulate this problem as a least-squares minimization problem, in which we define the cost functional

$$\mathcal{J}(\nu_e) = \frac{1}{2}\int_0^T \sum_{i=1}^N [m_i(t) - H_i\widetilde{w}(t, x; \nu_e)]^2 \, dt, \tag{2.12}$$

where N is the number of observation points, $H_i,\ i = 1, \ldots, N$ are operators which shall determine how we observe the solutions, and $m_i(t)$ are the measurements of our target field that we wish to reconstruct. We shall choose the operators $H_i,\ i = 1, \ldots, N$, such that

$$H_i : L^2(\Omega) \longrightarrow \mathbb{R}, \qquad i = 1, \ldots, N.$$

Thus, we wish to find the eddy viscosity $\check{\nu}$ such that

$$\check{\nu} = \underset{\nu_e \in H^3(\mathcal{L})}{\arg\min} \mathcal{J}(\nu_e). \tag{2.13}$$

To find the local minimizer of (2.12), we shall use a gradient-based optimization method. The optimal $\check{\nu}$ can be computed using a gradient descent algorithm as

$\check{\nu} = \lim_{n\to\infty} \nu^{(n)}$, where

$$\begin{cases} \nu^{(n+1)} & = \nu^{(n)} - \tau^{(n)}\, \nabla_{\nu_e} \mathcal{J}(\nu^{(n)}), \qquad n = 1, 2, \ldots, \\ \nu^{(1)} & = \nu_0, \end{cases} \tag{2.14}$$

in which $\nabla_{\nu_e}\mathcal{J}(\nu_e)$ is the gradient of the cost functional $\mathcal{J}(\nu_e)$ with respect to the control variable ν_e, $\tau^{(n)}$ is the n-iteration step length along the descent direction, and ν_0 is the initial guess for the eddy viscosity (which should be consistent with the Smagorinsky type ansatz).

2.3 Adjoint-Based Gradients

A key element of the minimization algorithm (2.14) is the gradient $\nabla_{\nu_e}\mathcal{J}(\nu_e)$. In order to determine it, we shall take the first variation of the functional in (2.12) with respect to ν_e. Computing the Gâteaux (directional) differential of the cost functional in (2.12)

$$\begin{aligned} \mathcal{J}'(\nu_e;\nu') &= \lim_{\epsilon\to 0} \frac{\mathcal{J}(\nu_e + \epsilon\nu') - \mathcal{J}(\nu_e)}{\epsilon}, \\ &= \frac{d}{d\epsilon}\, \mathcal{J}\Big(\nu_e + \epsilon\nu'\Big)\Big|_{\epsilon=0}, \\ &= \int_0^T \sum_{i=1}^{N} [H_i \widetilde{w}(t,x;\nu_e) - m_i(t)]\, H_i u'(t,x;\nu_e,\nu')\, dt, \end{aligned} \tag{2.15}$$

where the perturbation variable $u'(t,x;\nu_e,\nu')$ satisfies the perturbation system obtained from (2.8), and the perturbation variable $\nu'\big(\big(\frac{\partial\widetilde{w}}{\partial x}\big)^2\big)$ is the perturbation of

ν_e. The (local) minimizer of (2.12) requires the directional derivative of the cost functional to vanish for all perturbations ν', that is,

$$\underset{\nu' \in \Lambda(\mathcal{L})}{\forall} \qquad \mathcal{J}'(\check{\nu}; \nu') = 0, \tag{2.16}$$

where Λ is a suitable Hilbert space, to be specified below. For all other values of ν_e, we require a gradient with respect to ν_e in order to obtain the local minimizer $\check{\nu}$. To extract an expression for the gradient, we utilize the Riesz representation theorem and the fact that this is a directional derivative to obtain

$$\mathcal{J}'(\nu_e; \nu') = \left\langle \nabla_{\nu_e} \mathcal{J}, \nu' \right\rangle_{\Lambda(\mathcal{L})}, \tag{2.17}$$

where $\langle \cdot, \cdot \rangle_\Lambda$ is an inner product in the suitable Hilbert space Λ. To obtain the Riesz form in (2.17), we shall first note in (2.15) the multiplication between the two terms can be considered as an inner product over the reals, $\langle \cdot, \cdot \rangle_{\mathbb{R}}$, such that

$$\mathcal{J}'(\nu_e; \nu') = \int_0^T \sum_{i=1}^{N} \langle [H_i \widetilde{w}(t, x; \nu_e) - m_i(t)], H_i u'(t, x; \nu_e, \nu') \rangle_{\mathbb{R}} \, dt. \tag{2.18}$$

Written in terms of inner products, we can now use the suitable adjoint of the operators $H_i,\ i = 1, \ldots, N$, obtaining equivalent the inner product expressions for

(2.18)

$$\begin{aligned}\mathcal{J}'(\nu_e;\nu') &= \int_0^T \sum_{i=1}^{N} \langle [H_i\widetilde{w}(t,x;\nu_e) - m_i(t)], H_i u'(t,x;\nu_e,\nu')\rangle_{\mathbb{R}}\, dt,\\ &= \int_0^T \sum_{i=1}^{N} \langle H_i^*[H_i\widetilde{w}(t,x;\nu_e) - m_i(t)], u'(t,x;\nu_e,\nu')\rangle_{L^2(0,2\pi)}\, dt,\\ &= \int_0^T \int_0^{2\pi} \sum_{i=1}^{N} H_i^*[H_i\widetilde{w}(t,x;\nu_e) - m_i(t)]\, u'(t,x;\nu_e,\nu')\, dx\, dt, \qquad (2.19)\end{aligned}$$

where $H_i^*,\ i = 1,\ldots,N$, are the adjoint operators of the operators $H_i,\ i = 1,\ldots,N$. It is not yet possible to extract an expression for the gradient $\nabla_{\nu_e}\mathcal{J}(\nu_e)$ from the differential (2.19). The expression in (2.19) must hold for arbitrary perturbations $u'(t,x;\nu_e,\nu')$, which would require infinitely many test functions. Invoking the Riesz representation theorem to obtain (2.17), allows us to extract an expression for the gradient with respect to ν_e, independent of the arbitrary directions $\nu'(\left(\frac{\partial\widetilde{w}}{\partial x}\right)^2)$. We shall note that the perturbation variable ν' is hidden in the perturbation system that $u'(t,x;\nu_e,\nu')$, and the expression in (2.19) can be transformed to the Riesz form (2.17). Since the Riesz form given in (2.17) is not consistent the functional expression given in (2.19), we must prove that they are indeed equivalent. In the following theorem, we shall prove this and extract the expression for the gradient given in (2.17). This approach was initially formulated in [3], [2], and suitably modified for our current investigation.

Theorem 2.1. *Let $\nu' \in H^3(\mathcal{L})$. Then the directional differential in* (2.19) *has the*

following Riesz representation form

$$\mathcal{J}'(\nu;\nu') = \int_{s=a}^{b}\int_{t=0}^{T}\int_{x=0}^{2\pi} \frac{\partial \widetilde{u}^*(t,x)}{\partial x}\,\delta\Big(\Big(\frac{\partial \widetilde{u}(t,x)}{\partial x}\Big)^2 - s\Big)\,\frac{\partial^2}{\partial x^2}\Big(\sqrt{(s)}\Big)\,\nu'(s)\,dx\,dt\,ds, \tag{2.20}$$

where $\delta(\cdot)$ denotes the Dirac delta function and the adjoint variable $\widetilde{u}^*$ is defined as the solution to the system

$$\begin{aligned}
&-\frac{\partial \widetilde{u}^*}{\partial t} + \nu_1\frac{\partial^4 \widetilde{u}^*}{\partial x^4} + \nu_2\Big[\frac{\partial^2 \widetilde{u}^*}{\partial x^2} - \widetilde{u}\frac{\partial \widetilde{u}^*}{\partial x}\Big] \\
&\qquad + \frac{\partial}{\partial x}\Big[2\,\frac{d\nu}{d\big(\big(\frac{\partial \widetilde{u}}{\partial x}\big)^2\big)}\,\frac{\partial \widetilde{u}}{\partial x}\,\frac{\partial^3 \widetilde{u}}{\partial x^3}\,\frac{\partial \widetilde{u}^*}{\partial x}\Big] + \frac{\partial^3}{\partial x^3}\Big[\nu\,\frac{\partial \widetilde{u}^*}{\partial x}\Big] = \sum_{i=1}^{N} H_i^*[H_i\widetilde{u} - m_i], \\
&\frac{\partial^{(i)} \widetilde{u}^*}{\partial x^{(i)}}(t,0) = \frac{\partial^{(i)} \widetilde{u}^*}{\partial x^{(i)}}(t,2\pi), \qquad i = 0,\ldots,3, \\
&\widetilde{u}^*(T,x) = 0.
\end{aligned} \tag{2.21}$$

Proof. First, we must determine the perturbation of system (2.8), whose solution is

used in (2.19). This is done by perturbing the state variable $\widetilde{w}$ to obtain

$$\widetilde{w} = \widetilde{u} + \epsilon u' + \mathcal{O}(\epsilon^2), \tag{2.22a}$$

$$\frac{\partial \widetilde{w}}{\partial x} = \frac{\partial \widetilde{u}}{\partial x} + \epsilon \frac{\partial u'}{\partial x} + \mathcal{O}(\epsilon^2), \tag{2.22b}$$

$$\begin{aligned} \widetilde{w}\,\widetilde{w} &= (u + \epsilon u')\,(u + \epsilon u') + \mathcal{O}(\epsilon^2), \\ &= \widetilde{u}^2 + 2\epsilon \widetilde{u} u' + \mathcal{O}(\epsilon^2), \end{aligned} \tag{2.22c}$$

$$\begin{aligned} \Big(\frac{\partial \widetilde{w}}{\partial x}\Big)^2 &= \Big(\frac{\partial \widetilde{u}}{\partial x} + \epsilon \frac{\partial u'}{\partial x}\Big)^2 + \mathcal{O}(\epsilon^2), \\ &= \Big(\frac{\partial \widetilde{u}}{\partial x}\Big)^2 + 2\epsilon \frac{\partial \widetilde{u}}{\partial x}\,\frac{\partial u'}{\partial x} + \mathcal{O}(\epsilon^2), \end{aligned} \tag{2.22d}$$

$$\nu_e = \nu + \epsilon \nu' + \mathcal{O}(\epsilon^2). \tag{2.22e}$$

Since the viscosity term in (2.22e) depends on the state variable, let us expand the first term of the eddy viscosity separately in order to account for that. Determining the first term in (2.22e)

$$\begin{aligned} \nu\Big(\Big(\frac{\partial \widetilde{w}}{\partial x}\Big)^2\Big) &= \nu\Big(\Big(\frac{\partial \widetilde{u}}{\partial x} + \epsilon \frac{\partial u'}{\partial x}\Big)^2\Big) + \mathcal{O}(\epsilon^2), \\ &= \nu\Big(\Big(\frac{\partial \widetilde{u}}{\partial x}\Big)^2 + 2\epsilon \frac{\partial \widetilde{u}}{\partial x}\,\frac{\partial u'}{\partial x}\Big) + \mathcal{O}(\epsilon^2) \rightarrow \text{Taylor Expand}, \\ &= \nu\Big(\Big(\frac{\partial \widetilde{u}}{\partial x}\Big)^2\Big) + 2\epsilon\, \frac{d\big(\nu\big(\big(\frac{\partial \widetilde{u}}{\partial x}\big)^2\big)\big)}{d\big(\big(\frac{\partial \widetilde{u}}{\partial x}\big)^2\big)}\, \frac{\partial \widetilde{u}}{\partial x}\,\frac{\partial u'}{\partial x} + \mathcal{O}(\epsilon^2). \end{aligned} \tag{2.23}$$

Now we substitute (2.23) back into the eddy viscosity in (2.22e), to obtain the full

expression for the perturbation of the eddy viscosity

$$\begin{aligned}\nu_e\Big(\Big(\frac{\partial\widetilde{w}}{\partial x}\Big)^2\Big) &= \nu\Big(\Big(\frac{\partial\widetilde{w}}{\partial x}\Big)^2\Big) + \epsilon\nu'\Big(\Big(\frac{\partial\widetilde{w}}{\partial x}\Big)^2\Big) + \mathcal{O}(\epsilon^2),\\ &= \nu\Big(\Big(\frac{\partial\widetilde{u}}{\partial x}\Big)^2\Big) + 2\epsilon\,\frac{d\big(\nu\big(\big(\frac{\partial\widetilde{u}}{\partial x}\big)^2\big)\big)}{d\big(\big(\frac{\partial\widetilde{u}}{\partial x}\big)^2\big)}\frac{\partial\widetilde{u}}{\partial x}\frac{\partial u'}{\partial x} + \epsilon\nu'\Big(\Big(\frac{\partial\widetilde{w}}{\partial x}\Big)^2\Big) + \mathcal{O}(\epsilon^2). \quad (2.24)\end{aligned}$$

Using these perturbations, we can calculate the nonlinear model term, given in (2.7), for the perturbed version of (2.8), truncating at $\mathcal{O}(\epsilon^2)$

$$\begin{aligned}\nu_e\Big(\Big(\frac{\partial\widetilde{w}}{\partial x}\Big)^2\Big)\frac{\partial^3\widetilde{w}}{\partial x^3} &= \Big(\nu + 2\epsilon\,\frac{d\nu}{d\big(\big(\frac{\partial\widetilde{u}}{\partial x}\big)^2\big)}\frac{\partial\widetilde{u}}{\partial x}\frac{\partial u'}{\partial x} + \epsilon\nu'\Big)\Big(\frac{\partial^3\widetilde{u}}{\partial x^3} + \epsilon\frac{\partial^3 u'}{\partial x^3}\Big) + \mathcal{O}(\epsilon^2),\\ &= \nu\,\frac{\partial^3\widetilde{u}}{\partial x^3} + \epsilon\Big[2\,\frac{d\nu}{d\big(\big(\frac{\partial\widetilde{u}}{\partial x}\big)^2\big)}\frac{\partial u'}{\partial x}\frac{\partial\widetilde{u}}{\partial x}\frac{\partial^3\widetilde{u}}{\partial x^3} + \nu'\frac{\partial^3\widetilde{u}}{\partial x^3} + \nu\frac{\partial^3 u'}{\partial x^3}\Big] + \mathcal{O}(\epsilon^2). \quad (2.25)\end{aligned}$$

Substituting the expressions in (2.22) and (2.25) into (2.8), and collecting to the order of $\mathcal{O}(\epsilon)$, we obtain the perturbation system

$$\begin{aligned}\frac{\partial u'}{\partial t} + \nu_1\frac{\partial^4 u'}{\partial x^4} + \nu_2\Big[\frac{\partial^2 u'}{\partial x^2} + \frac{\partial(\widetilde{u}u')}{\partial x}\Big] &= -\frac{\partial}{\partial x}\Big[\Big(2\frac{d\nu}{d\Big(\big(\frac{\partial\widetilde{u}}{\partial x}\big)^2\Big)}\frac{\partial\widetilde{u}}{\partial x}\frac{\partial u'}{\partial x} + \nu'\Big)\frac{\partial^3\widetilde{u}}{\partial x^3} + \nu\frac{\partial^3 u'}{\partial x^3}\Big],\\ \frac{\partial^{(i)}u'}{\partial x^{(i)}}(t,0) &= \frac{\partial^{(i)}u'}{\partial x^{(i)}}(t,2\pi), \qquad i = 0,\ldots,3,\\ u'(0,x) &= 0. \quad (2.26)\end{aligned}$$

We shall note that $\widetilde{w} = \widetilde{u}$ at leading order, so we now adopt the convection that $\widetilde{u} = \widetilde{w}$, representing the LES field. Similarly, $\nu_e\big(\big(\frac{\partial\widetilde{w}}{\partial x}\big)^2\big) = \nu\big(\big(\frac{\partial\widetilde{w}}{\partial x}\big)^2\big)$ at leading order, so we denote $\nu\big(\big(\frac{\partial\widetilde{u}}{\partial x}\big)^2\big) = \nu_e\big(\big(\frac{\partial\widetilde{w}}{\partial x}\big)^2\big)$ as the eddy viscosity.

Now we integrate (2.26) against the adjoint field $\widetilde{u}^*$ over space and time

$$\begin{aligned}
&\int_0^T \int_0^{2\pi} \left[\frac{\partial u'}{\partial t} + \nu_1 \frac{\partial^4 u'}{\partial x^4} + \nu_2 \Big[\frac{\partial^2 u'}{\partial x^2} + \frac{\partial(\widetilde{u}\, u')}{\partial x} \Big] \right] \widetilde{u}^* \, dx \, dt \\
&\quad = - \int_0^T \int_0^{2\pi} \left[\frac{\partial}{\partial x} \Big[\left(2 \frac{d\nu}{d\big(\big(\frac{\partial \widetilde{u}}{\partial x}\big)^2\big)} \frac{\partial \widetilde{u}}{\partial x} \frac{\partial u'}{\partial x} + \nu' \right) \frac{\partial^3 \widetilde{u}}{\partial x^3} + \nu \frac{\partial^3 u'}{\partial x^3} \Big] \right] \widetilde{u}^* \, dx \, dt. \qquad (2.27)
\end{aligned}$$

Let us consider the second term in (2.27) by using integration by parts with respect to space

$$\begin{aligned}
&- \int_0^T \int_0^{2\pi} \left[\frac{\partial}{\partial x} \Big[\left(2 \frac{d\nu}{d\big(\big(\frac{\partial \widetilde{u}}{\partial x}\big)^2\big)} \frac{\partial \widetilde{u}}{\partial x} \frac{\partial u'}{\partial x} + \nu' \right) \frac{\partial^3 \widetilde{u}}{\partial x^3} + \nu \frac{\partial^3 u'}{\partial x^3} \Big] \right] \widetilde{u}^* \, dx \, dt \\
&= \int_0^T \left[- \Big[\left(2 \frac{d\nu}{d\big(\big(\frac{\partial \widetilde{u}}{\partial x}\big)^2\big)} \frac{\partial \widetilde{u}}{\partial x} \frac{\partial u'}{\partial x} + \nu' \right) \frac{\partial^3 \widetilde{u}}{\partial x^3} \widetilde{u}^* + \nu \frac{\partial^3 u'}{\partial x^3} \widetilde{u}^* \Big] \Big|_{x=0}^{2\pi} \right. \\
&\quad \left. + \int_0^{2\pi} \Big[\left(2 \frac{d\nu}{d\big(\big(\frac{\partial \widetilde{u}}{\partial x}\big)^2\big)} \frac{\partial \widetilde{u}}{\partial x} \frac{\partial u'}{\partial x} + \nu' \right) \frac{\partial^3 \widetilde{u}}{\partial x^3} + \nu \frac{\partial^3 u'}{\partial x^3} \Big] \frac{\partial \widetilde{u}^*}{\partial x} dx \right] dt.
\end{aligned}$$

From (2.11) we know that ν is periodic in x, thus we also know that its perturbation ν' is also periodic in x. Using this fact, as well as (2.8), (2.11), (2.26), and (2.21), the boundary term vanishes and we are left with

$$\begin{aligned}
&- \int_0^T \int_0^{2\pi} \left[\frac{\partial}{\partial x} \Big[\left(2 \frac{d\nu}{d\big(\big(\frac{\partial \widetilde{u}}{\partial x}\big)^2\big)} \frac{\partial \widetilde{u}}{\partial x} \frac{\partial u'}{\partial x} + \nu' \right) \frac{\partial^3 \widetilde{u}}{\partial x^3} + \nu \frac{\partial^3 u'}{\partial x^3} \Big] \right] \widetilde{u}^* \, dx \, dt \\
&= \int_0^T \int_0^{2\pi} \Big[\left(2 \frac{d\nu}{d\big(\big(\frac{\partial \widetilde{u}}{\partial x}\big)^2\big)} \frac{\partial \widetilde{u}}{\partial x} \frac{\partial u'}{\partial x} + \nu' \right) \frac{\partial^3 \widetilde{u}}{\partial x^3} + \nu \frac{\partial^3 u'}{\partial x^3} \Big] \frac{\partial \widetilde{u}^*}{\partial x} \, dx \, dt. \qquad (2.28)
\end{aligned}$$

Substituting (2.28) back into (2.27), we obtain a slightly simpler relation to work

with, namely,

$$\int_0^T \int_0^{2\pi} \left[\frac{\partial u'}{\partial t} + \nu_1 \frac{\partial^4 u'}{\partial x^4} + \nu_2 \Big[\frac{\partial^2 u'}{\partial x^2} + \frac{\partial(\widetilde{u}u')}{\partial x} \Big] \right] \widetilde{u}^* \, dx \, dt$$
$$= \int_0^T \int_0^{2\pi} \Big[\Big(2 \frac{d\nu}{d\big(\big(\frac{\partial \widetilde{u}}{\partial x}\big)^2\big)} \frac{\partial \widetilde{u}}{\partial x} \frac{\partial u'}{\partial x} + \nu' \Big) \frac{\partial^3 \widetilde{u}}{\partial x^3} + \nu \frac{\partial^3 u'}{\partial x^3} \Big] \frac{\partial \widetilde{u}^*}{\partial x} \, dx \, dt. \tag{2.29}$$

Now, we can rearrange (2.29) such that the terms containing the perturbation variable u' are on the left-hand side (LHS) and terms containing the perturbation variable ν' are on the right-hand side (RHS). Doing this, we obtain

$$\int_0^T \int_0^{2\pi} \left[\frac{\partial u'}{\partial t} + \nu_1 \frac{\partial^4 u'}{\partial x^4} + \nu_2 \Big[\frac{\partial^2 u'}{\partial x^2} + \frac{\partial(\widetilde{u}u')}{\partial x} \Big] \right] \widetilde{u}^*$$
$$- \left[2 \frac{d\nu}{d\big(\big(\frac{\partial \widetilde{u}}{\partial x}\big)^2\big)} \frac{\partial \widetilde{u}}{\partial x} \frac{\partial u'}{\partial x} \frac{\partial^3 \widetilde{u}}{\partial x^3} + \nu \frac{\partial^3 u'}{\partial x^3} \right] \frac{\partial \widetilde{u}^*}{\partial x} \, dx \, dt$$
$$= \int_0^T \int_0^{2\pi} \frac{\partial \widetilde{u}^*}{\partial x} \frac{\partial^3 \widetilde{u}}{\partial x^3} \nu' \, dx \, dt. \tag{2.30}$$

Now, we can perform integration by parts individually on each of the terms on the LHS of (2.30) to extract all the terms with u'. After performing integration by parts, while using the relations from (2.11), the boundary conditions, and the time domain

conditions from (2.8), (2.26), and (2.21), we obtain the following relation

$$\begin{aligned}
&\int_0^T \int_0^{2\pi} \Big[\frac{\partial u'}{\partial t} + \nu_1 \frac{\partial^4 u'}{\partial x^4} + \nu_2 \Big[\frac{\partial^2 u'}{\partial x^2} + \frac{\partial(\widetilde{u}\, u')}{\partial x} \Big] \Big] \widetilde{u}^* \\
&\quad - \Big[\, 2 \frac{d\nu}{d\big(\big(\frac{\partial \widetilde{u}}{\partial x}\big)^2\big)} \frac{\partial \widetilde{u}}{\partial x} \frac{\partial u'}{\partial x} \frac{\partial^3 \widetilde{u}}{\partial x^3} + \nu \frac{\partial^3 u'}{\partial x^3} \, \Big] \frac{\partial \widetilde{u}^*}{\partial x} \, dx \, dt \\
&= \int_0^T \int_0^{2\pi} \Big[- \frac{\partial \widetilde{u}^*}{\partial t} + \nu_1 \frac{\partial^4 \widetilde{u}^*}{\partial x^4} + \nu_2 \Big[\frac{\partial^2 \widetilde{u}^*}{\partial x^2} - \widetilde{u} \frac{\partial \widetilde{u}^*}{\partial x} \Big] \\
&\quad + \frac{\partial}{\partial x} \Big[2 \frac{d\nu}{d\big(\big(\frac{\partial \widetilde{u}}{\partial x}\big)^2\big)} \frac{\partial \widetilde{u}}{\partial x} \frac{\partial^3 \widetilde{u}}{\partial x^3} \frac{\partial \widetilde{u}^*}{\partial x} \Big] + \frac{\partial^3}{\partial x^3} \Big[\nu \frac{\partial \widetilde{u}^*}{\partial x} \Big] \Big] u' \, dx \, dt \\
&= \int_0^T \int_0^{2\pi} \frac{\partial \widetilde{u}^*}{\partial x} \frac{\partial^3 \widetilde{u}}{\partial x^3} \nu' \, dx \, dt.
\end{aligned}$$

Using the expression for the adjoint system in (2.21) and the expression for the directional differential in (2.19), we obtain

$$\begin{aligned}
&\int_0^T \int_0^{2\pi} \Big[- \frac{\partial \widetilde{u}^*}{\partial t} + \nu_1 \frac{\partial^4 \widetilde{u}^*}{\partial x^4} + \nu_2 \Big[\frac{\partial^2 \widetilde{u}^*}{\partial x^2} - \widetilde{u} \frac{\partial \widetilde{u}^*}{\partial x} \Big] \\
&\quad + \frac{\partial}{\partial x} \Big[2 \frac{d\nu}{d\big(\big(\frac{\partial \widetilde{u}}{\partial x}\big)^2\big)} \frac{\partial \widetilde{u}}{\partial x} \frac{\partial^3 \widetilde{u}}{\partial x^3} \frac{\partial \widetilde{u}^*}{\partial x} \Big] + \frac{\partial^3}{\partial x^3} \Big[\nu \frac{\partial \widetilde{u}^*}{\partial x} \Big] \Big] u' \, dx \, dt \\
&= \int_0^T \int_0^{2\pi} \Big[\sum_{i=1}^{N} H_i^* [H_i \widetilde{u} - m_i] \Big] u' dx dt = \int_0^T \int_0^{2\pi} \frac{\partial \widetilde{u}^*}{\partial x} \frac{\partial^3 \widetilde{u}}{\partial x^3} \nu' \, dx \, dt, \\
&= \mathcal{J}'(\nu; \nu').
\end{aligned} \tag{2.31}$$

Note the last expression given in (2.31) has integration over space and time. In order to put the expression into the Riesz form given in (2.17), we require the integration to be over the state variable $s = (\frac{\partial \widetilde{u}}{\partial x})^2$. To do this, let us introduce the following

representations

$$\begin{aligned} h\Big(\Big(\frac{\partial \widetilde{u}}{\partial x}\Big)^2\Big) &:= \frac{\partial^3 \widetilde{u}}{\partial x^3}, \\ &= \frac{\partial^2}{\partial x^2}\Big(\frac{\partial \widetilde{u}}{\partial x}\Big), \\ &= \frac{\partial^2}{\partial x^2}\Big(\sqrt{\Big(\frac{\partial \widetilde{u}}{\partial x}\Big)^2}\Big), \end{aligned} \tag{2.32}$$

$$f\Big(\Big(\frac{\partial \widetilde{u}}{\partial x}\Big)^2\Big) = \int_{-\infty}^{\infty} \delta\Big(\Big(\frac{\partial \widetilde{u}}{\partial x}\Big)^2 - s\Big)\, f(s) ds, \tag{2.33}$$

where δ is the Dirac delta function. We have performed the change in (2.32) to simply show that we can write the third derivative as a function of the state variable. The transformation in (2.33) is a utilization of the "sifting" property of the Dirac delta function, to introduce the integration over the state variable. Now, we can let f be equal to the terms in (2.31) that depend on the state variable

$$\begin{aligned} f\Big(\Big(\frac{\partial \widetilde{u}}{\partial x}\Big)^2\Big) &= \frac{\partial^3 \widetilde{u}}{\partial x^3}\, \nu'\Big(\Big(\frac{\partial \widetilde{u}}{\partial x}\Big)^2\Big), \\ &= h\Big(\Big(\frac{\partial \widetilde{u}}{\partial x}\Big)^2\Big)\, \nu'\Big(\Big(\frac{\partial \widetilde{u}}{\partial x}\Big)^2\Big), \\ &= \int_{-\infty}^{\infty} \delta\Big(\Big(\frac{\partial \widetilde{u}}{\partial x}\Big)^2 - s\Big)\, h(s)\, \nu'(s)\, ds. \end{aligned} \tag{2.34}$$

Now we use (2.34) in (2.31)

$$\begin{aligned}
\mathcal{J}'(\nu;\nu') &= \int_0^T \int_0^{2\pi} \frac{\partial \widetilde{u}^*}{\partial x} \frac{\partial^3 \widetilde{u}}{\partial x^3} \nu'\Big(\Big(\frac{\partial \widetilde{u}}{\partial x}\Big)^2\Big)\, dx\, dt, \\
&= \int_0^T \int_0^{2\pi} \frac{\partial \widetilde{u}^*}{\partial x} \int_a^b \delta\Big(\Big(\frac{\partial \widetilde{u}}{\partial x}\Big)^2 - s\Big)\, h(s)\, \nu'(s)\, ds\, dx\, dt, \\
&= \int_0^T \int_0^{2\pi} \int_a^b \frac{\partial \widetilde{u}^*}{\partial x}\, \delta\Big(\Big(\frac{\partial \widetilde{u}}{\partial x}\Big)^2 - s\Big)\, h(s)\, \nu'(s)\, ds\, dx\, dt.
\end{aligned}$$

Using Fubini's theorem to swap the order of integration,

$$\begin{aligned}
\mathcal{J}'(\nu;\nu') &= \int_0^T \int_0^{2\pi} \int_a^b \frac{\partial \widetilde{u}^*}{\partial x}\, \delta\Big(\Big(\frac{\partial \widetilde{u}}{\partial x}\Big)^2 - s\Big)\, h(s)\, \nu'(s)\, ds\, dx\, dt, \\
&= \int_a^b \int_0^T \int_0^{2\pi} \frac{\partial \widetilde{u}^*}{\partial x}\, \delta\Big(\Big(\frac{\partial \widetilde{u}}{\partial x}\Big)^2 - s\Big)\, h(s)\, \nu'(s)\, dx\, dt\, ds, \\
&= \int_{s=a}^b \int_{t=0}^T \int_{x=0}^{2\pi} \frac{\partial \widetilde{u}^*(t,x)}{\partial x}\, \delta\Big(\Big(\frac{\partial \widetilde{u}(t,x)}{\partial x}\Big)^2 - s\Big)\, \frac{\partial^2}{\partial x^2}\Big(\sqrt{(s)}\Big)\, \nu'(s)\, dx\, dt\, ds, \qquad (2.35) \\
&= \langle \nabla_\nu \mathcal{J}, \nu' \rangle_{L^2(\mathcal{L})},
\end{aligned}$$

we obtain the Riesz representation form given in (2.20) and the differential of the cost functional in the Riesz form given in (2.17). □

Now we have the differential of the cost functional in the Riesz representation form so that we can determine the cost functional gradients in different Hilbert spaces

Λ. Currently, we have the simple form of the $L^2(\mathcal{L})$ gradient

$$\begin{aligned}\nabla_\nu^{L^2}\mathcal{J}(s) &= \int_{t=0}^{T}\int_{x=0}^{2\pi} \frac{\partial\widetilde{u}^*(t,x)}{\partial x}\,\delta\Big(\Big(\frac{\partial\widetilde{u}(t,x)}{\partial x}\Big)^2 - s\Big)\,\frac{\partial^2}{\partial x^2}\Big(\sqrt{(s)}\Big)\,dx\,dt,\\ &= \int_{t=0}^{T}\int_{x=0}^{2\pi} \frac{\partial\widetilde{u}^*(t,x)}{\partial x}\,\delta\Big(\Big(\frac{\partial\widetilde{u}(t,x)}{\partial x}\Big)^2 - s\Big)\,\frac{\partial^3\widetilde{u}(t,x)}{\partial x^3}\,dx\,dt. \end{aligned} \tag{2.36}$$

We can simplify this gradient expression so that it is easier to evaluate by using the Heaviside function

$$\chi_{[a,b]}(s) = \begin{cases} 1, & s \in [a,b],\\ 0, & s \notin [a,b], \end{cases}$$

instead of the Dirac Delta distribution. We shall write

$$\delta\Big(\Big(\frac{\partial\widetilde{u}(t,x)}{\partial x}\Big)^2 - s\Big) = -\frac{d}{ds}\chi_{[\alpha,(\frac{\partial\widetilde{u}(t,x)}{\partial x})^2]}(s). \tag{2.37}$$

Then, using (2.37) in (2.36) we can further simplify the gradient expression

$$\begin{aligned}\nabla_\nu^{L^2}\mathcal{J}(s) &= \int_{t=0}^{T}\int_{x=0}^{2\pi} \frac{\partial\widetilde{u}^*(t,x)}{\partial x}\,\delta\Big(\Big(\frac{\partial\widetilde{u}(t,x)}{\partial x}\Big)^2 - s\Big)\,\frac{\partial^2}{\partial x^2}\Big(\sqrt{(s)}\Big)\,dx\,dt,\\ &= \int_{t=0}^{T}\int_{x=0}^{2\pi} \frac{\partial\widetilde{u}^*(t,x)}{\partial x}\,\delta\Big(\Big(\frac{\partial\widetilde{u}(t,x)}{\partial x}\Big)^2 - s\Big)\,\frac{\partial^3\widetilde{u}(t,x)}{\partial x^3}\,dx\,dt,\\ &= \int_{t=0}^{T}\int_{x=0}^{2\pi} -\frac{d}{ds}\chi_{[\alpha,(\frac{\partial\widetilde{u}(t,x)}{\partial x})^2]}(s)\,\frac{\partial\widetilde{u}^*(t,x)}{\partial x}\,\frac{\partial^3\widetilde{u}(t,x)}{\partial x^3}\,dx\,dt,\\ &= -\frac{d}{ds}\int_{t=0}^{T}\int_{x=0}^{2\pi} \chi_{[\alpha,(\frac{\partial\widetilde{u}(t,x)}{\partial x})^2]}(s)\,\frac{\partial\widetilde{u}^*(t,x)}{\partial x}\,\frac{\partial^3\widetilde{u}(t,x)}{\partial x^3}\,dx\,dt. \end{aligned} \tag{2.38}$$

Since we require the eddy viscosity to be $\nu \in H^3(\mathcal{L})$, we need the gradients to be

sufficiently smooth for the eddy viscosity to have this level of smoothness. Thus, the L^2 gradient is not sufficiently smooth to use. Instead, we shall use the Sobolev space H^3, to ensure regularity of the gradients and of the resulting eddy viscosity. So we set $\Lambda = H^3(\mathcal{L})$, where $H^3(\mathcal{L})$ is the Sobolev space endowed with the inner product

$$
\begin{aligned}
&\langle p_1, p_2 \rangle_{H^3(\mathcal{L})}, \\
&= \Big\langle p_1, p_2 \Big\rangle_{L^2(\mathcal{L})} + l_1^2 \Big\langle \frac{dp_1}{ds}, \frac{p_2}{ds} \Big\rangle_{L^2(\mathcal{L})} + l_2^4 \Big\langle \frac{d^2p_1}{ds^2}, \frac{p_2}{ds^2} \Big\rangle_{L^2(\mathcal{L})} + l_3^6 \Big\langle \frac{d^3p_1}{ds^3}, \frac{p_2}{ds^3} \Big\rangle_{L^2(\mathcal{L})}, \\
&= \int_{s=a}^{b} \left[p_1\, p_2 + l_1^2 \frac{dp_1}{ds}\frac{dp_2}{ds} + l_2^4 \frac{d^2p_1}{ds^2}\frac{d^2p_2}{ds^2} + l_3^6 \frac{d^3p_1}{ds^3}\frac{d^3p_2}{ds^3} \right] ds,
\end{aligned}
$$

where $p_1, p_2 \in H^3(\mathcal{L})$, $l_1, l_2, l_3 \in \mathbb{R}$ are the length scale parameters for each of the respective inner products that increase the regularity. As long as the length scale parameters

$$0 < l_1, l_2, l_3 < \infty,$$

we have equivalent inner products (in the sense of norm equivalence). That is, invoking the Riesz representation theorem we obtain for the directional derivative

$$
\begin{aligned}
\mathcal{J}'(\nu;\nu') &= \langle \nabla_\nu^{L^2} \mathcal{J}, \nu' \rangle_{L^2(\mathcal{L})}, \\
&= \langle \nabla_\nu^{H^3} \mathcal{J}, \nu' \rangle_{H^3(\mathcal{L})}, \\
&= \Big\langle \nabla_\nu^{H^3} \mathcal{J}, \nu' \Big\rangle_{L^2(\mathcal{L})} + l_1^2 \Big\langle \frac{d(\nabla_\nu^{H^3} \mathcal{J})}{ds}, \frac{d\nu'}{ds} \Big\rangle_{L^2(\mathcal{L})} + l_2^4 \Big\langle \frac{d^2(\nabla_\nu^{H^3} \mathcal{J})}{ds^2}, \frac{d^2\nu'}{ds^2} \Big\rangle_{L^2(\mathcal{L})} \\
&\quad + l_3^6 \Big\langle \frac{d^3(\nabla_\nu^{H^3} \mathcal{J})}{ds^3}, \frac{d^3\nu'}{ds^3} \Big\rangle_{L^2(\mathcal{L})}, \qquad (2.39)
\end{aligned}
$$

Just as before, we wish to isolate the perturbation term which we shall do by using integration by parts. Before we begin computing the inner products in (2.39), we must assume boundary conditions for the Sobolev gradient $\nabla_\nu^{H^3}\mathcal{J}$

$$\frac{d^{(2i+1)}\left(\nabla_\nu^{H^3}\mathcal{J}\right)}{ds^{(2i+1)}}\Big|_{s=a} = \frac{d^{(i)}\left(\nabla_\nu^{H^3}\mathcal{J}\right)}{ds^{(i)}}\Big|_{s=b} = 0, \qquad i = 0, \ldots, 2. \tag{2.40}$$

Since we are looking at the set of functions $\nabla_\nu^{H^3}\mathcal{J}$ that must satisfy the boundary conditions (2.40), we must also consider the set of functions ν' which inherit these constraints. Now, let us observe the first term in (2.39)

$$\left\langle \nabla_\nu^{H^3}\mathcal{J}, \nu' \right\rangle_{L^2(\mathcal{L})} = \int_{s=a}^{b} \nabla_\nu^{H^3}\mathcal{J}\,\nu'\,ds. \tag{2.41}$$

This term is already in the appropriate form, so we do not need to perform integration by parts. Now we consider the second term in (2.39)

$$\left\langle \frac{d(\nabla_\nu^{H^3}\mathcal{J})}{ds}, \frac{d\nu'}{ds} \right\rangle_{L^2(\mathcal{L})} = \int_{s=a}^{b} \frac{d(\nabla_\nu^{H^3}\mathcal{J})}{ds}\,\frac{d\nu'}{ds}\,ds.$$

Performing integration by parts, and using the boundary condition in (2.40)

$$\begin{aligned}
\left\langle \frac{d(\nabla_\nu^{H^3}\mathcal{J})}{ds}, \frac{d\nu'}{ds} \right\rangle_{L^2(\mathcal{L})} &= \int_{s=a}^{b} \frac{d(\nabla_\nu^{H^3}\mathcal{J})}{ds}\,\frac{d\nu'}{ds}\,ds, \\
&= \left[\frac{d(\nabla_\nu^{H^3}\mathcal{J})}{ds}\,\nu'\right]\Big|_{s=a}^{b} - \int_{s=a}^{b} \frac{d^2(\nabla_\nu^{H^3}\mathcal{J})}{ds^2}\,\nu'\,ds, \\
&= -\int_{s=a}^{b} \frac{d^2(\nabla_\nu^{H^3}\mathcal{J})}{ds^2}\,\nu'\,ds.
\end{aligned} \tag{2.42}$$

Similarly, we use integration by parts and the boundary conditions in (2.40) to

transform the third term in (2.39)

$$\begin{aligned}
\Big\langle \frac{d^2(\nabla_\nu^{H^3}\mathcal{J})}{ds^2}, \frac{d^2\nu'}{ds^2} \Big\rangle_{L^2(\mathcal{L})} &= \int_{s=a}^{b} \frac{d^2(\nabla_\nu^{H^3}\mathcal{J})}{ds^2}\,\frac{d^2\nu'}{ds^2}\,ds, \\
&= \Big[\frac{d^2(\nabla_\nu^{H^3}\mathcal{J})}{ds^2}\,\frac{d\nu'}{ds}\Big]\Big|_{s=a}^{b} - \int_{s=a}^{b} \frac{d^3(\nabla_\nu^{H^3}\mathcal{J})}{ds^3}\,\frac{d\nu'}{ds}\,ds, \\
&= -\Big[\frac{d^3(\nabla_\nu^{H^3}\mathcal{J})}{ds^3}\,\nu'\Big]\Big|_{s=a}^{b} + \int_{s=a}^{b} \frac{d^4(\nabla_\nu^{H^3}\mathcal{J})}{ds^4}\,\nu'\,ds, \\
&= \int_{s=a}^{b} \frac{d^4(\nabla_\nu^{H^3}\mathcal{J})}{ds^4}\,\nu'\,ds. \qquad (2.43)
\end{aligned}$$

Lastly, we perform integration by parts on the fourth term in (2.39) and use the boundary conditions in (2.40)

$$\begin{aligned}
\Big\langle \frac{d^3(\nabla_\nu^{H^3}\mathcal{J})}{ds^3}, \frac{d^3\nu'}{ds^3} \Big\rangle_{L^2(\mathcal{L})} &= \int_{s=a}^{b} \frac{d^3(\nabla_\nu^{H^3}\mathcal{J})}{ds^3}\,\frac{d^3\nu'}{ds^3}\,ds, \\
&= \Big[\frac{d^3(\nabla_\nu^{H^3}\mathcal{J})}{ds^3}\,\frac{d^2\nu'}{ds^2}\Big]\Big|_{s=a}^{b} - \int_{s=a}^{b} \frac{d^4(\nabla_\nu^{H^3}\mathcal{J})}{ds^4}\,\frac{d^2\nu'}{ds^2}\,ds, \\
&= -\Big[\frac{d^4(\nabla_\nu^{H^3}\mathcal{J})}{ds^4}\,\frac{d\nu'}{ds}\Big]\Big|_{s=a}^{b} + \int_{s=a}^{b} \frac{d^5(\nabla_\nu^{H^3}\mathcal{J})}{ds^5}\,\frac{d\nu'}{ds}\,ds, \\
&= \Big[\frac{d^5(\nabla_\nu^{H^3}\mathcal{J})}{ds^5}\,\nu'\Big]\Big|_{s=a}^{b} - \int_{s=a}^{b} \frac{d^6(\nabla_\nu^{H^3}\mathcal{J})}{ds^6}\,\nu'\,ds, \\
&= -\int_{s=a}^{b} \frac{d^6(\nabla_\nu^{H^3}\mathcal{J})}{ds^6}\,\nu'\,ds. \qquad (2.44)
\end{aligned}$$

When performing integration by parts, the only terms that remain are the integrals over the space domain, and all boundary terms are zero due to the (judiciously chosen) boundary conditions in (2.40). Now plugging the expressions found in (2.41),

(2.42), (2.43), and (2.44) into (2.39), we obtain

$$\begin{aligned}\langle \nabla_\nu^{L^2}\mathcal{J},\nu'\rangle_{L^2(\mathcal{L})} &= \langle \nabla_\nu^{H^3}\mathcal{J},\nu'\rangle_{H^3(\mathcal{L})},\\ &= \left\langle \nabla_\nu^{H^3}\mathcal{J},\nu'\right\rangle_{L^2(\mathcal{L})} + l_1^2\left\langle \frac{d(\nabla_\nu^{H^3}\mathcal{J})}{ds},\frac{d\nu'}{ds}\right\rangle_{L^2(\mathcal{L})}\\ &\quad + l_2^4\left\langle \frac{d^2(\nabla_\nu^{H^3}\mathcal{J})}{ds^2},\frac{d^2\nu'}{ds^2}\right\rangle_{L^2(\mathcal{L})} + l_3^6\left\langle \frac{d^3(\nabla_\nu^{H^3}\mathcal{J})}{ds^3},\frac{d^3\nu'}{ds^3}\right\rangle_{L^2(\mathcal{L})},\end{aligned}$$

$$= \int_{s=a}^{b}\left[\nabla_\nu^{H^3}\mathcal{J} - l_1^2\cdot\frac{d^2(\nabla_\nu^{H^3}\mathcal{J})}{ds^2} + l_2^4\cdot\frac{d^4(\nabla_\nu^{H^3}\mathcal{J})}{ds^4} - l_3^6\cdot\frac{d^6(\nabla_\nu^{H^3}\mathcal{J})}{ds^6}\right]\nu'\,ds. \quad (2.45)$$

Since this integral relation must hold for every arbitrary ν', then determining the Sobolev gradient reduces down to solving the inhomogeneous elliptic boundary value problem

$$\nabla_\nu^{L^2}\mathcal{J}(s) = \nabla_\nu^{H^3}\mathcal{J}(s) - l_1^2\,\frac{d^2(\nabla_\nu^{H^3}\mathcal{J}(s))}{ds^2} + l_2^4\,\frac{d^4(\nabla_\nu^{H^3}\mathcal{J}(s))}{ds^4} - l_3^6\,\frac{d^6(\nabla_\nu^{H^3}\mathcal{J}(s))}{ds^6}, \quad (2.46a)$$

$$\frac{d^{(2i+1)}\left(\nabla_\nu^{H^3}\mathcal{J}(s)\right)}{ds^{(2i+1)}}\Big|_{s=a} = \frac{d^{(i)}\left(\nabla_\nu^{H^3}\mathcal{J}(s)\right)}{ds^{(i)}}\Big|_{s=b} = 0, \qquad i=0,\ldots,2. \quad (2.46b)$$

It should be noted that other boundary condition choices in (2.46b) can be made to determine the Sobolev gradients, but the present boundary values were found to best suit the current investigation. The left boundary condition allows the values of $\nu\big(\big(\frac{\partial\widetilde{u}}{\partial x}\big)^2\big)$ at $s=a$ to change, otherwise this would fix the assumption $\nu\big(\big(\frac{\partial\widetilde{u}}{\partial x}\big)^2\big)=0$ at $s=0$ (from the Smagorinsky ansatz). Where-as, the right boundary condition fixes the values at $s=b$. Since $\mathcal{I}\subset\mathcal{L}$, we have $b>\mathcal{I}$ for all identifiability intervals.

So, the value of $\nu\big(\big(\frac{\partial \widetilde{u}}{\partial x}\big)^2\big)$ at $s = b$ will not be required when solving the LES system, hence we can fix the value at $s = b$. These boundary conditions are a design choice, and will inherently effect the general characteristics of the eddy viscosity near the endpoints $s = a$ and $s = b$.

By adjusting the length scale parameters l_1, l_2, l_3, we effectively control the smoothness of the Sobolev gradient $\nabla_\nu^{H^3}\mathcal{J}(s)$, and the smoothness of the optimal eddy viscosity. We can consider the differential equation (2.46) in Fourier space, to obtain

$$\begin{aligned}
\nabla_\nu^{L^2}\mathcal{J} &= \nabla_\nu^{H^3}\mathcal{J} - l_1^2\,\frac{d^2(\nabla_\nu^{H^3}\mathcal{J})}{ds^2} + l_2^4\,\frac{d^4(\nabla_\nu^{H^3}\mathcal{J})}{ds^4} - l_3^6\,\frac{d^6(\nabla_\nu^{H^3}\mathcal{J})}{ds^6},\\
\nabla_\nu^{L^2}\mathcal{J} &= \left(I - l_1^2\,\frac{d^2}{ds^2} + l_2^4\,\frac{d^4}{ds^4} - l_3^6\,\frac{d^6}{ds^6}\right)\nabla_\nu^{H^3}\mathcal{J},\\
\widehat{\nabla_\nu^{L^2}\mathcal{J}} &= \left(1 + l_1^2\,k^2 + l_2^4\,k^4 + l_3^6\,k^6\right)\widehat{\nabla_\nu^{H^3}\mathcal{J}},\\
\widehat{\nabla_\nu^{H^3}\mathcal{J}} &= \underbrace{\frac{1}{1 + l_1^2\,k^2 + l_2^4\,k^4 + l_3^6\,k^6}}_{L(k)}\,\widehat{\nabla_\nu^{L^2}\mathcal{J}}.
\end{aligned} \tag{2.47}$$

We can see that as the length scale parameters l_1, l_2, l_3, increase, the function $L(k)$ acts as a more aggressive "low-pass" filter applied to the L^2 gradient. The higher indexed length scale parameters have a higher influence on the filtering process due to the high powers on the wavenumbers. These parameters shall act as "knobs" we can adjust in order to obtain a sufficiently smooth eddy viscosity. We also note if the length scale parameters are all set equal to zero, we simply obtain the original L^2 gradient.

Chapter 3

Problem Set-up

In our current investigation, there are several factors that can intrinsically change the behaviour of the given flow and the properties of the optimization procedure. In this chapter, we discuss the physical parameters to be used for solving our DNS and LES solutions. The observation operators are also introduced, which allows us to minimize the cost functional in the physical space.

3.1 Physical Parameters

In order to determine an optimal eddy viscosity, we must select physical parameters that could intrinsically change the evolution of the solutions to the governing system. One way that we can control the behaviour of the Kuramoto-Sivashinsky equations is by choosing particular values of the dissipation and energy production terms, ν_1 and ν_2 respectively, first introduced in (1.6). If we consider the linear terms of (1.6),

and take the Fourier transform with respect to x, we obtain

$$\begin{aligned}
&\frac{\partial u(t,x)}{\partial t} + \nu_1 \frac{\partial^4 u(t,x)}{\partial x^4} + \nu_2 \frac{\partial^2 u(t,x)}{\partial x^2} = 0,\\
&\frac{\partial \hat{u}(t,k)}{\partial t} + \nu_1 k^4 \hat{u}(t,k) - \nu_2 k^2 \hat{u}(t,k) = 0,\\
&\frac{\partial \hat{u}(t,k)}{\partial t} = \underbrace{k^2\left[\nu_2 - \nu_1 k^2\right]}_{F(k)} \hat{u}(t,k).
\end{aligned} \tag{3.1}$$

Considering the RHS of (3.1) as a general function of coefficients $F(k)$, dependent on wavenumber k, we can determine the maximum/ peak wavenumber of the system. Taking the derivative of $F(k)$ with respect to k, and setting it equal to 0

$$\begin{aligned}
0 &= \frac{dF}{dk},\\
0 &= 2k\left[\nu_2 - \nu_1 k^2\right] + k^2\left[-2\nu_1 k\right],\\
0 &= \nu_2 - 2\nu_1 k^2,\\
|k| &= \sqrt{\frac{\nu_2}{2\nu_1}}.
\end{aligned} \tag{3.2}$$

From (3.2), we can see that $F(k)$ peaks at a wavenumber determined by ν_1 and ν_2. This wavenumber corresponds to the number of crests we should (on average) observe in the solution. For our numerical results we set $\nu_1 = 1$ and $\nu_2 = 100$, so using (3.2) we expect

$$\begin{aligned}
|k| &= \sqrt{\frac{100}{2}},\\
&\approx 7,
\end{aligned}$$

crests to be present in the solutions. Since the solution spectrum peaks around this wavenumber, we choose a Fourier filter cutoff k_{max} in (2.2) larger than this value to ensure that majority of the energy is captured in the spectrum when performing the LES. So for the numerical results provided, we set the maximum resolved wavenumber $k_{max} = 16$.

The number of observation points, N in (2.12), shall be chosen to be less than the number of resolved Fourier modes in the LES. Thus, we set $N = 8$ as the number of observation points. To obtain an appropriate initial condition $w_0(x)$ for the system, we begin with a simple initial condition of $-\sin(x)$. We use this sine function as an initial condition in (1.6), and solve the DNS system for an extended period of time such that this particular initial condition is "forgotten" and the turbulent dynamics of the system are present in the solution. We then take this final turbulent solution as the initial condition $w(0, x) = w_0(x)$ which we shall use in computations of the DNS and LES. It shall also be noted that choosing the initial condition in this manner ensures that we obtain solutions with a "full" spectrum. Using this as our initial condition at $t = 0$, we choose a terminal time value $T = 3 \times 10^{-3}$. This is long enough to include a few characteristic "events" in the system evolution, however without a closure term the solutions will not completely diverge from the DNS or become unbounded.

For (2.14), we must use an appropriate Smagorinsky-type initial guess for the eddy viscosity ν_0. For this, we shall use

$$\nu_0\Big(\Big(\frac{\partial \widetilde{u}}{\partial x}\Big)^2\Big) = (C_s\, k_{max})^2 \left(\sqrt{\Big(\frac{\partial \widetilde{u}}{\partial x}\Big)^2}\right), \tag{3.3}$$

where C_s is the Smagorinsky coefficient.

3.2 Observation Operator

For this current investigation, we shall choose to minimize the cost functional defined in the physical space at some (equispaced) points, $\{x_i\}_{i=1}^{N=8}$. Thus the operators $H_i,\ i = 1, \ldots, N$ acting on the function g will be expressed in terms of integration against a Dirac Delta function δ, such that

$$H_i g = \int_0^{2\pi} \delta(x_i - x)\, g(x)\, dx, \qquad i = 1, \ldots, N. \tag{3.4}$$

We must also determine the corresponding adjoint of the operators, $H_i^*,\ i = 1, \ldots, N$, which is required to obtain the form given in (2.19). Since

$$H_i : L^2(\Omega) \longrightarrow \mathbb{R}, \qquad i = 1, \ldots, N, \tag{3.5}$$

we shall consider the following

$$\begin{aligned} &g_1 \in \mathbb{R}, \qquad g_2 \in L^2(\Omega), \\ &H_i : L^2(\Omega) \longrightarrow \mathbb{R}, && i = 1, \ldots, N, \\ &H_i g_2 = \int_0^{2\pi} \delta(x_i - x)\, g_2(x)\, dx, && i = 1, \ldots, N. \end{aligned}$$

Now solving the adjoint operator H_i^*

$$\begin{aligned}\langle g_1, H_i g_2\rangle_{\mathbb{R}} &= g_1 \int_0^{2\pi} \delta(x_i - x)\, g_2(x)\, dx, \\ &= \int_0^{2\pi} \left[\delta(x_i - x)\, g_1\right]\, g_2(x)\, dx, \\ &= \langle H_i^* g_1, g_2\rangle_{L^2(\Omega)}, \qquad i = 1, \ldots, N.\end{aligned}$$

We note that the operators $H_i,\ i = 1, \ldots, N$ are not self-adjoint ($H_i \neq H_i^*$), but we obtain an alternate mapping for $H_i^*,\ i = 1, \ldots, N$

$$\begin{aligned} &H_i^* : \mathbb{R} \longrightarrow L^2(\Omega), && i = 1, \ldots, N, \\ &H_i^* = \delta(x_i - x), && i = 1, \ldots, N.\end{aligned}$$

Chapter 4

Numerical Approach

The purpose of this chapter is to describe the numerical approach used for solving our optimization problem. The numerical techniques for solving the PDEs and numerically dealing with the state dependent eddy viscosity is discussed. The gradient descent approach used in this problem is also introduced, and sequence of steps for constructing the optimal eddy viscosity is outlined.

4.1 Discretization

Now that we have formulated the optimization problem in the continuous setting, we shall discretize the problem numerically to approximate the optimal eddy viscosity. For this problem, we are dealing with PDEs, which naturally must be discretized over the spatial and temporal domain. Since the control variable, $\nu\left(\left(\frac{\partial \widetilde{u}}{\partial x}\right)^2\right)$, is dependent on the state (flow) variable, we must also consider a domain over this state dependent domain. That means we must create numerical grids for: $x \in (0, 2\pi)$, $t \in [0, T]$,

and $\left(\frac{\partial \widetilde{u}}{\partial x}\right)^2 \in \mathcal{L}$. For all calculations, we attempt to use spectrally accurate numerical methods to maintain optimal accuracy of solutions, while still being computationally efficient. The domain Ω will be discretized using N_x equispaced grid points, such that the step-size in space shall be denoted as Δx. Similarly, we denote Δt as the step-size in time. Chebyshev points are used to discretize the state space, which will allow us to utilize several spectrally accurate methods. As described in [26], the Chebyshev points are

$$\gamma_n = \cos\left(\frac{n\,\pi}{N_s}\right), \quad \text{for} \quad n = 0, \ldots, N_s,$$

where N_s is the number of points used to discretize the state domain. We notice that $\gamma_n \in [-1, 1]$, so we must rescale the state domain. Noting the width of the state domain

$$W = \frac{b-a}{2},$$

and the midpoint of the domain

$$M = \frac{a+b}{2},$$

we can easily shift and rescale the Chebyshev points to our state domain

$$\begin{aligned} s_n &= \frac{1}{2}\left[a + b + (b-a)\,\gamma_n\right], \\ &= M + W\,\gamma_n. \end{aligned}$$

We can also compute the corresponding rescaling for differentiation/ integration in the state space

$$ds_n = W\, d\gamma_n,$$
$$d\gamma_n = \frac{1}{W}\, ds_n.$$

When computing derivatives in state space, $\frac{d\nu}{d\left(\left(\frac{\partial \bar{u}}{\partial x}\right)^2\right)}$ (such as in (2.21) or in (2.38)), we can use Chebyshev differentiation as described in [26], and rescale appropriately for our domain. Similarly, when required to integrate in the state space (such as in Section 5.3) we use the Clenshaw-Curtis quadrature also described in [26], and appropriately scale the integration weighting. Both methods described ensure we have spectral accuracy, to minimize errors in the state domain. It should also be noted, that when performing integration in the periodic spatial domain, we use the trapezoidal numerical integration, which on the periodic domain is equivalent to the Gauss quadrature.

To solve the stiff partial differential equations given in (1.6), (2.8), and (2.21) we utilize the exponential time-differencing fourth-order Runge-Kutta method (ETDRK4) introduced in [6] but we shall use the modified version from [14]. With this method, we obtain spectral accuracy in the spatial domain and fourth order accuracy in the temporal domain, $\mathcal{O}(\Delta t^4)$. It should be noted that the system of equations given in (1.6) and (2.8) are initial-value problems, so we integrate forwards in time. Where as, the adjoint system given in (2.21) is a terminal-value problem, so we must integrate backwards in time. This can be easily modified to be an initial-value problem, such

that we can use the ETDRK4 method, via the simple substitution

$$\dot{t} = T - t.$$

Then, computationally we solve the following adjoint system forwards in time

$$\begin{aligned}
&\frac{\partial \widetilde{u}^*}{\partial t} + \nu_1 \frac{\partial^4 \widetilde{u}^*}{\partial x^4} + \nu_2 \Big[\frac{\partial^2 \widetilde{u}^*}{\partial x^2} - \widetilde{u} \frac{\partial \widetilde{u}^*}{\partial x} \Big] \\
&\qquad + \frac{\partial}{\partial x} \Big[2 \frac{d\nu}{d\big(\big(\frac{\partial \widetilde{u}}{\partial x} \big)^2 \big)} \frac{\partial \widetilde{u}}{\partial x} \frac{\partial^3 \widetilde{u}}{\partial x^3} \frac{\partial \widetilde{u}^*}{\partial x} \Big] + \frac{\partial^3}{\partial x^3} \Big[\nu \frac{\partial \widetilde{u}^*}{\partial x} \Big] = \sum_{i=1}^{N} H_i^* [H_i \widetilde{u} - m_i], \\
&\frac{\partial^{(i)} \widetilde{u}^*}{\partial x^{(i)}}(t, 0) = \frac{\partial^{(i)} \widetilde{u}^*}{\partial x^{(i)}}(t, 2\pi), \qquad i = 0, \ldots, 3, \\
&\widetilde{u}^*(0, x) = 0.
\end{aligned}$$

When solving the fully resolved (DNS) system in (1.6), we use standard dealiasing and the Orszag Two-Thirds Rule [1], to obtain alias-free results for the DNS. For the filtered systems, LES and adjoint system in (2.8) and (2.21) respectively, we are not required to dealias given that the aggressive filtering operation has an effect equivalent to dealiasing. In addition, we shall note that the standard 2/3 rule would not appropriately dealias these equations. This is due to the product of more than two terms appearing in the equations, as well as the 2/3 rule holds for only polynomial terms and the form of the eddy viscosity is unknown [1].

In solving the partial differential equations there is a dependence on the eddy viscosity and its derivative, which are defined in the state space. Since we are solving these equations in the x domain, we require a way to define the eddy viscosity and

its derivative in terms of the x domain. To do this, we use barycentric interpolation on Chebyshev points [27]. This method ensures that our eddy viscosity and its derivatives remain sufficiently smooth, while maintaining accuracy. This form of the barycentric interpolation also ensures that the interpolation remains stable and is computationally efficient for the given domains.

To obtain a spectrally accurate solution for the Sobolev gradient, we use the `Chebfun` package [10] to solve the ordinary differential equation given in (2.46). The `Chebfun` package (with the use of ultraspherical polynomials) allows us to solve this high-order boundary-value problem, in a computationally efficient manner without having to adjust for ill-conditioned matrices. Since all methods are implemented using spectrally accurate approaches, except for time-stepping, we expect time-stepping ($\mathcal{O}(\Delta t^4)$) to be the dominating error term in computations for solving the differential equations and determining the gradient.

4.2 Gradient Descent

Once we have computed the appropriate Sobolev gradient, we must iteratively compute the optimal eddy viscosity, via (2.14). Rather than naively using the basic form of the steepest descent method, we further improve the approach by using a conjugate gradient method. In particular, we use the Polak-Ribiere formula [19] to construct a favourable descent direction. This method constructs a conjugate descent direction that uses information from the previous descent direction in order to optimize next

direction taken. The Polak-Ribiere method uses a factor to determine the magnitude that the previous gradient effects the current gradient, computed using the formula

$$\gamma_{PR} = \frac{\left\langle \left(g_{n+1} - g_n\right), g_{n+1} \right\rangle_{\Lambda(\mathcal{L})}}{\left\langle g_n, g_n \right\rangle_{\Lambda(\mathcal{L})}}, \tag{4.1}$$

where

$$g_{n+1} = -\nabla_\nu \mathcal{J}(\nu^{(n+1)}).$$

The conjugate direction is then determined by

$$\nabla_\nu \mathcal{J}(\nu^{(n+1)}) = g_{n+1} + \gamma_{PR}\, g_n. \tag{4.2}$$

It shall be noted that when we compute the conjugate gradient for the nth iteration, this replaces the previously computed value. When choosing to compute the conjugate gradient, this can be determined with respect the L^2 gradient or the H^3 gradient. In this investigation, we choose to determine the Sobolev gradient, then construct the conjugate gradient using $\nabla_\nu^{H^3}\mathcal{J}$. Initially, $\gamma_{PR} = 0$ and after f_{PR} iterations the value of γ_{PR} is reset to 0. This resets the conjugate gradient method, which has been found to ensure the method does not "run out of steam" [19].

We also need to determine the optimal step length $\tau^{(n)}$, in (2.14), to ensure we do not take too small or large of a step when applying the gradient. We solve this by

determining at each iteration

$$\tau^{(n)} = \arg\max_{\tau>0}\{\mathcal{J}(\tau) = \mathcal{J}(\nu^{(n)} - \tau\,\nabla_\nu \mathcal{J}(\nu^{(n)}))\}. \tag{4.3}$$

To perform this, we use a bracketing routine along with Brent's method [19], in a nonlinear minimization function. This method does not require derivatives, so it determines the optimal step length in a computationally efficient manner. So, we use the sequence of steps outlined in Algorithm 1 to obtain the optimal eddy viscosity.

Algorithm 1 Algorithm for constructing optimal eddy viscosity $\check{\nu}$

- set $n = 0$
- set ν_0 as a Smagorinsky type initial guess

repeat

- set $n = n + 1$
- solve the direct LES problem in (2.8)
- solve the adjoint problem in (2.21)
- determine the cost functional gradient $\nabla_\nu^{L^2}\mathcal{J}(\nu^{(n)})$ given by (2.38)
- determine the Sobolev gradient $\nabla_\nu^{H^3}\mathcal{J}(\nu^{(n)})$ given by (2.38)
- determine the conjugate gradient, using the Polak-Ribiere method given in (4.1) and (4.2)
- determine the optimal step length $\tau^{(n)}$ in (2.14), by solving (4.3) via Brent's line minimization method
- update the eddy viscosity $\nu^{(n)}$, using the gradient descent algorithm (2.14)

until condition termination criterion for optimal $\nu^{(n)}$ is satisfied

The algorithm terminates once the cost functional gradient can no longer be reduced, which computationally we implement by imposing the condition on the relative difference of the cost functional values per iteration

$$\frac{|\mathcal{J}(\nu^{(n+1)}) - \mathcal{J}(\nu^{(n)})|}{\mathcal{J}(\nu^{(n)})} < \epsilon_{tol}, \tag{4.4}$$

where ϵ_{tol} is tolerance criterion.

Chapter 5

Results

This chapter highlights the key numerical results, obtained from this investigation. We state the diagnostic quantities used to determine the performance of multiple numerical solutions. A fundamental test for validating the gradient used to determine the optimal eddy viscosity is studied, to ensure calculations were performed correctly. The numerical results are shown, and key cases for particular values of the Sobolev parameters are investigated.

5.1 Numerical Parameters

Solving this highly sensitive optimization problem, several numerical parameters were tested to ensure numerical methods were stable and converged to appropriate solutions. To solve the required PDEs, $N_x = 1024 = 2^{10}$ points were used to discretize the spatial domain, giving a step-size of $\Delta x \approx 6.1359 \times 10^{-3}$. We use a temporal step size of $\Delta t = 3.0 \times 10^{-6}$, which ensures that accurate solutions to the PDEs

are obtained. To encompass the entire range of the state variable, numerically we set $\mathcal{L} := [a = 0, b = 400^2]$. The interval $\mathcal{L}$ was discretized using $N_s = 4096 = 2^{12}$ Chebyshev points, and the eddy viscosity was discretized on the fixed interval $\mathcal{L}$ using these points. For the initial guess of the eddy viscosity, we set the Smagorinsky coefficient equal to $C_s = 0.002$. The resetting frequency for the conjugate gradient method used was $f_{PR} = 10$, and we set the termination tolerance $\epsilon_{tol} = 10^{-7}$.

5.2 Diagnostic Quantities

In order to assess how well the optimal eddy viscosity performs and how close the predictions of our LES models are to the DNS solutions, in this section we introduce several diagnostic quantities. The first quantity we shall use is

$$E_1(t) = \frac{1}{||w(t)||_{L^2(0,2\pi)}||\widetilde{u}(t)||_{L^2(0,2\pi)}} \int_0^{2\pi} w(t,x)\,\widetilde{u}(t,x)\; dx. \tag{5.1}$$

This diagnostic quantity could be considered as the cosine of the "angle" between the DNS and LES solutions, computed at each point in time. The second diagnostic quantity we shall consider is the L^2 difference between the DNS and LES solutions, normalized by the "exact" solution (DNS), which is given as

$$E_2(t) = \frac{1}{||w(t)||^2_{L^2(0,2\pi)}} \int_0^{2\pi} \left(w(t,x) - \widetilde{u}(t,x)\right)^2 dx. \tag{5.2}$$

We shall also introduce 3 different diagnostic quantities, pertaining particularly to the energy in the system. We shall consider the kinetic energy, normalized by the

kinetic energy of the DNS

$$\begin{aligned} K(t) &= \frac{||\widetilde{u}(t)||^2_{L^2(0,2\pi)}}{||w(t)||^2_{L^2(0,2\pi)}}, \\ &= \frac{1}{||w(t)||^2_{L^2(0,2\pi)}} \int_0^{2\pi} \widetilde{u}(t,x)^2 \, dx. \end{aligned} \tag{5.3}$$

The normalized enstrophy (H^1 seminorm), shall also be observed

$$\begin{aligned} E_3(t) &= \frac{|\widetilde{u}(t)|^2_{H^1(0,2\pi)}}{|w(t)|^2_{H^1(0,2\pi)}}, \\ &= \frac{1}{|w(t)|^2_{H^1(0,2\pi)}} \int_0^{2\pi} \left(\frac{\partial \widetilde{u}(t,x)}{\partial x} \right)^2 dx, \end{aligned} \tag{5.4}$$

where $|\cdot|^2_{H^p}$ denotes the seminorm

$$|v|^2_{H^p(\Pi)} = ||\nabla^p v||^2_{L^2(\Pi)} = \int_\Pi \left(\frac{\partial^p v}{\partial x^p} \right)^2 dx.$$

The third energy diagnostic quantity we consider is the normalized H^2 seminorm

$$\begin{aligned} E_4(t) &= \frac{|\widetilde{u}(t)|^2_{H^2(0,2\pi)}}{|w(t)|^2_{H^2(0,2\pi)}}, \\ &= \frac{1}{|w(t)|^2_{H^2(0,2\pi)}} \int_0^{2\pi} \left(\frac{\partial^2 \widetilde{u}(t,x)}{\partial x^2} \right)^2 dx. \end{aligned} \tag{5.5}$$

We shall now note the relationship between rate of change of the kinetic energy with the H^1 and H^2 seminorms. To do this, we consider the Kuramoto-Sivashinsky

equation

$$\frac{\partial u}{\partial t} + \nu_1 \frac{\partial^4 u}{\partial x^4} + \nu_2 \left[\frac{\partial^2 u}{\partial x^2} + u \frac{\partial u}{\partial x}\right] = 0,$$
$$\frac{\partial u}{\partial t} = -\nu_1 \frac{\partial^4 u}{\partial x^4} - \nu_2 \left[\frac{\partial^2 u}{\partial x^2} + u \frac{\partial u}{\partial x}\right]. \tag{5.6}$$

Now we integrate (5.6) against u over space

$$\int_0^{2\pi} u \frac{\partial u}{\partial t}\, dx = \int_0^{2\pi} -u \left[\nu_1 \frac{\partial^4 u}{\partial x^4} + \nu_2 \left[\frac{\partial^2 u}{\partial x^2} + u \frac{\partial u}{\partial x}\right]\right] dx,$$
$$\frac{d}{dt} \int_0^{2\pi} \frac{1}{2} u^2\, dx = -\nu_1 \int_0^{2\pi} u \frac{\partial^4 u}{\partial x^4}\, dx - \nu_2 \int_0^{2\pi} u \frac{\partial^2 u}{\partial x^2}\, dx - \nu_2 \int_0^{2\pi} u^2 \frac{\partial u}{\partial x}\, dx. \tag{5.7}$$

The LHS of (5.7) is simply the time derivative of the kinetic energy. Now we shall perform integration by parts on the third term on the RHS of (5.7), to show the nonlinear term does not contribute energy to the system

$$\int_0^{2\pi} u^2 \frac{\partial u}{\partial x}\, dx = \int_0^{2\pi} u^2 \frac{\partial u}{\partial x}\, dx,$$
$$= \left[u^3\right] \Big|_{x=0}^{2\pi} - 2 \int_0^{2\pi} u^2 \frac{\partial u}{\partial x}\, dx. \tag{5.8}$$

Due to the periodic boundary conditions, the first term in (5.8) is equal to zero. Thus, we have

$$\begin{aligned}
\int_0^{2\pi} u^2 \frac{\partial u}{\partial x}\, dx &= -2 \int_0^{2\pi} u^2 \frac{\partial u}{\partial x}\, dx, \\
3 \int_0^{2\pi} u^2 \frac{\partial u}{\partial x}\, dx &= 0, \\
\int_0^{2\pi} u^2 \frac{\partial u}{\partial x}\, dx &= 0.
\end{aligned} \tag{5.9}$$

Therefore, we can see from (5.9) that the nonlinear term is equal to zero, and does not contribute energy into the system. So, we perform integration parts on the remaining (linear) terms on the RHS of (5.7)

$$\begin{aligned}
\frac{dK_{kin}(t)}{dt} &= -\nu_1 \int_0^{2\pi} u \frac{\partial^4 u}{\partial x^4}\, dx - \nu_2 \int_0^{2\pi} u \frac{\partial^2 u}{\partial x^2}\, dx, \\
\frac{dK_{kin}(t)}{dt} &= -\nu_1 \int_0^{2\pi} \left(\frac{\partial^2 u}{\partial x^2} \right)^2 dx + \nu_2 \int_0^{2\pi} \left(\frac{\partial u}{\partial x} \right)^2 dx, \\
\frac{dK_{kin}(t)}{dt} &= \nu_2 \left| u(t) \right|^2_{H^1(0,2\pi)} - \nu_1 \left| u(t) \right|^2_{H^2(0,2\pi)}.
\end{aligned} \tag{5.10}$$

From (5.10), we can see that the rate of change with respect to time of the kinetic energy consists of simply the H^1 seminorm minus the H^2 seminorm, scaled by ν_2 and ν_1 respectively. The final diagnostic quantity we shall consider is the error history at the observation points

$$\{x_i\}_{i=1}^{N=8} = \left\{ (i-1)\frac{\pi}{4} \right\}_{i=1}^{8}. \tag{5.11}$$

We use the following normalization factor for the observation error history

$$F = \frac{1}{2\pi T} \int_0^T \int_0^{2\pi} w(t,x)^2 \, dx \, dt, \tag{5.12}$$

to give a reference magnitude of the "true" solution. So, we shall consider the difference between the LES and DNS at each individual observation point

$$E_{x_i}(t) = \frac{1}{F} \left(w(t,x_i) - \widetilde{u}(t,x_i) \right)^2, \qquad i = 1, \ldots, N. \tag{5.13}$$

5.3 Validation of Gradient Evaluation

Due to the mathematical and computational complexity of determining the key element of the gradient descent algorithm in (2.14), cost functional gradient $\nabla_\nu \mathcal{J}(\nu)$, we shall now introduce a validation method to ensure this gradient will be computed correctly. Denoted the κ-test, this is a diagnostic test to verify that the gradient of the cost functional is computed correctly. This consists of comparing the directional derivative in (2.17) using two forms, one being the Gâteaux derivative approximated using the finite-difference and the other is the expression for $\mathcal{J}'$ given in terms of the Riesz representation formula and the adjoint-based gradient, given in (2.17). We take the quotient of these these two quantities to obtain the κ-test

$$\kappa(\epsilon) = \frac{\epsilon^{-1}[\mathcal{J}(\nu + \epsilon\nu') - \mathcal{J}(\nu)]}{\langle \nabla_\nu \mathcal{J}, \nu' \rangle_{\Lambda(\mathcal{L})}}, \tag{5.14}$$

where ϵ is the magnitude of the perturbation in the direction of ν', for discretizing the finite difference formulation of the directional derivative. Since these expressions should be equivalent, we expect the values of $\kappa(\epsilon)$ to be close to unity, which confirms that the gradient has been computed correctly. However, we should note for large values of ϵ we expect a poor finite difference approximation. In addition, for small values of ϵ numerical round-off will become of concern causing cancellation errors. Thus, we expect the value of κ to be close to unity for an intermediate range of ϵ values. We also note that the denominator in (5.14) can be evaluated using different Hilbert spaces Λ, hence, we shall only verify the L^2 gradient since the Sobolev gradient $\nabla_\nu^{H^3}\mathcal{J}$ is a smoother version of $\nabla_\nu^{L^2}\mathcal{J}$, so we should put more emphasis on validating the L^2 gradient. Therefore, computationally we shall verify our gradient by checking

$$\kappa(\epsilon) = \frac{\epsilon^{-1}[\mathcal{J}(\nu+\epsilon\nu') - \mathcal{J}(\nu)]}{\int_{s=a}^{b} \nabla_\nu^{L^2}\mathcal{J}(s)\,\nu'(s)\,ds} \approx 1. \tag{5.15}$$

Since this directional derivative is defined for arbitrary perturbations and should hold for any function in that space, we expect the expression in (5.15) to hold for any $\nu'(s)$. Thus, it is also important to perform this test using multiple test functions $\nu'\big(\big(\frac{\partial\widetilde{u}}{\partial x}\big)^2\big)$.

For mathematical and computational purposes, we shall test two random perturbations

$$\nu_1'(s) = 10^{-2}\left(4\cos\left(\frac{s}{350000}\right)\right)^2, \tag{5.16}$$

$$\nu_2'(s) = 2 - \left(\exp\left(\frac{s}{750000}\right)\right)^2. \tag{5.17}$$

We perform the κ-test for these test functions, with a range of $\epsilon \in [10^{-15}, 10^{-1}]$. The results in Figure 5.1 show the values of $\kappa(\epsilon)$ and in Figure 5.2 we observe how close to unity the values of the κ-test are. As expected, for intermediate values of ϵ the value of $\kappa(\epsilon)$ is very close to unity. Also as anticipated, we notice for very small values and large values of ϵ, $\kappa(\epsilon)$ deviates away from unity, which is due to numerical round-off errors and a poor finite difference approximation respectively. We shall also note in Figure 5.2, as numerical parameters are refined the values $\kappa(\epsilon)$ tends closer to unity, which is the expected trend.

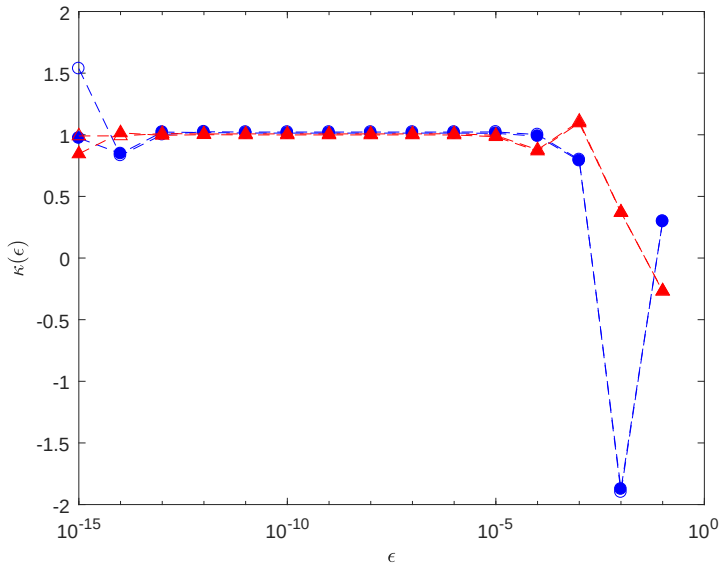

Figure 5.1: The values of $\kappa(\epsilon)$ given in (5.15), for the perturbations (5.16) (blue, circles) and (5.17) (red, triangles), using two numerical time step values: $\Delta t = 3 \times 10^{-6}$ (empty symbol) and $\Delta t = 1 \times 10^{-6}$ (filled symbol).

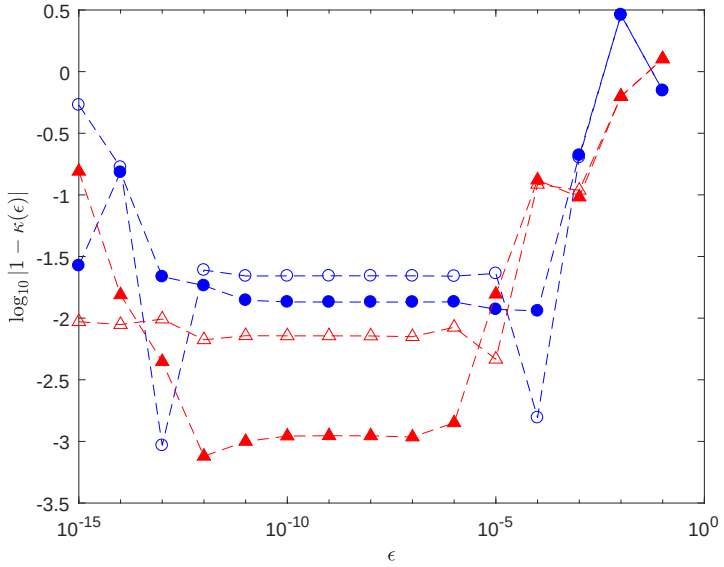

Figure 5.2: The quantity $\log_{10}|1 - \kappa(\epsilon)|$, for the perturbations (5.16) (blue, circles) and (5.17) (red, triangles), using two numerical time step values: $\Delta t = 3 \times 10^{-6}$ (empty symbol) and $\Delta t = 1 \times 10^{-6}$ (filled symbol).

5.4 Computational Results

We begin with a few plots to help understand the dynamics of the given flow. In Figure 5.4, we provide a plot of the spectrum of the initial condition $w_0(x)$ used for these computations. In Figures 5.5, 5.6, and 5.7, we provide space-time contour plots of the DNS, LES with no closure term, and LES with the closure given in terms initial guess ν_0, to see the intrinsic behaviour of each of the flows. In Figure 5.5, we can see the interesting characteristic "events" as the merging and separation of the peaks of the solution. Figures 5.4 and 5.5 also indicate the maximum resolved wavenumber $k_{max} = 16$, representing the filter in Fourier and physical space respectively.

Solving the minimization problem (2.13) to determine the optimal eddy viscosity $\check{\nu}$, we use the Sobolev length-scale parameters l_1, l_2, l_3 to ensure the eddy viscosity is sufficiently smooth as well as to optimize the convergence to $\check{\nu}$ in (2.14). For simplicity, we set $l_1 = 0$ and adjust the values of l_2 and l_3. In Figure 5.3, we show a schematic of the function $L(k)$ given in (2.47). We can see how the "low-pass" filter acts as a function of the Sobolev length-scale parameters, and how we can make this more aggressive by increasing the Sobolev length scale parameter to act upon lower wavenumbers. Due to the steep slope the filter has for l_2 and l_3, these dominate the filtering process and this is why we can simply set $l_1 = 0$. In Figure 5.8, we show the value of the cost functional for various Sobolev parameters and in Figure 5.9 show the corresponding optimal eddy viscosity compared to the initial guess given in (3.3). The value of the cost functional (2.12) for the initial guess was $\mathcal{J}(\nu_0) = 1.4823$. In Table 5.1, we have provided multiple cases with corresponding Sobolev parameters and cost functional value at the optimal eddy viscosity $\check{\nu}$. Several combinations of

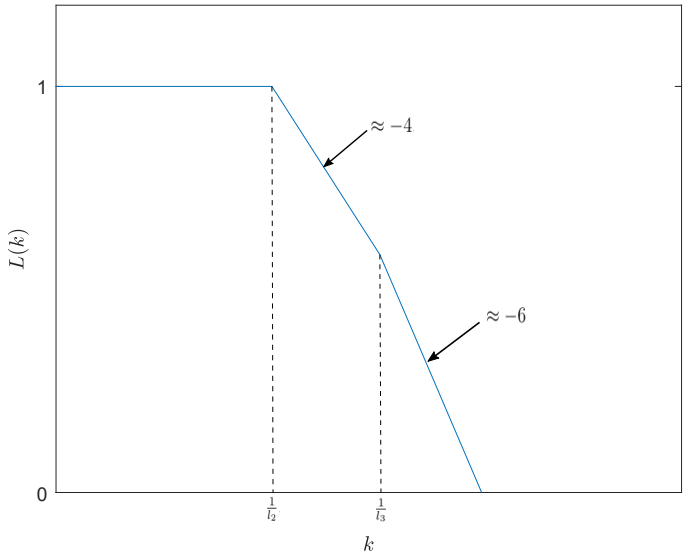

Figure 5.3: Schematic of the function $L(k)$ given in (2.47), in log-based coordinates for $l_2 > l_3$. Noted are $\frac{1}{l_2}$ and $\frac{1}{l_3}$, with the slope the of the resulting filter being ≈ -4 and ≈ -6, respectively.

Sobolev parameters were tested, and the cases shown in Table 5.1 were found to best minimize the cost functional in the optimization procedure.

Choosing the two best representative cases, we wish to apply our diagnostic tools in order to measure how well the corresponding optimal closures perform within and beyond the optimization window T. So, we test the optimal eddy viscosities for a time interval up to $t = 2T$ and compare the result of four cases: DNS, LES with no closure, LES with the closure given in terms initial guess ν_0, and the LES with the optimal eddy viscosity $\check{\nu}$. We use the LES with no closure comparison, as a way of observing how the system behaves solely based on the large-scale structures. Observing this solution also serves as a verification that we have chosen an aggressive enough filter such that the solution diverges from the DNS. Observing the solution of the LES

with the closure given in terms initial guess ν_0 will act as a reference solution for the standard Smagorinsky model, which we expect the optimal eddy viscosity solution to improve upon. First, we shall consider the optimal eddy viscosity $\check{\nu}$ obtained from Case C given in Table 5.1. We choose to observe Case C, because it reduces the cost functional by a factor of ≈ 4.4 while producing a very smooth eddy viscosity (as shown below). We show: a space-time contour plot in Figure 5.10(a), first diagnostic quantity $E_1(t)$ from (5.1) in Figure 5.11(a), second diagnostic quantity $E_2(t)$ from (5.2) in Figure 5.12(a), normalized kinetic energy $K(t)$ from (5.3) in Figure 5.13(a), normalized enstrophy $E_3(t)$ from (5.4) in Figure 5.14(a), normalized H^2 seminorm $E_4(t)$ from (5.5) in Figure 5.15(a), and the observation point error normalized $E_{x_i}(t)$ from (5.13) in Figure 5.16. We also compare the solutions in physical space in Figure 5.18.

The optimal eddy viscosity obtained from Case D given in Table 5.1 obtains the smallest value of $\mathcal{J}$, and so we use it as the second representative case to apply our diagnostic tools. We show: a space-time contour plot in Figure 5.10(b), first diagnostic quantity $E_1(t)$ from (5.1) in Figure 5.11(b), second diagnostic quantity

Case	$\mathbf{l_1}$	$\mathbf{l_2}$	$\mathbf{l_3}$	$\mathcal{J}(\check{\nu})$	**Notes**
A	0	10^6	10^6	0.4313	
B	0	10^1	10^5	0.4313	
C	0	10^4	10^3	0.3347	smooth dependence of $\check{\nu}$ on $\left(\frac{\partial \widetilde{u}}{\partial x}\right)^2$
D	0	10^3	10^1	0.1806	rough dependence of $\check{\nu}$ on $\left(\frac{\partial \widetilde{u}}{\partial x}\right)^2$

Table 5.1: A summary of the optimal eddy viscosities, for different Sobolev parameters l_1, l_2, l_3. The corresponding value of the cost functional is provided.

$E_2(t)$ from (5.2) in Figure 5.12(b), normalized kinetic energy $K(t)$ from (5.3) in Figure 5.13(b), normalized enstrophy $E_3(t)$ from (5.4) in Figure 5.14(b), normalized H^2 seminorm $E_4(t)$ from (5.5) in Figure 5.15(b), and the observation point error normalized $E_{x_i}(t)$ from (5.13) in Figure 5.17. We also compare the solutions in physical space in Figure 5.19.

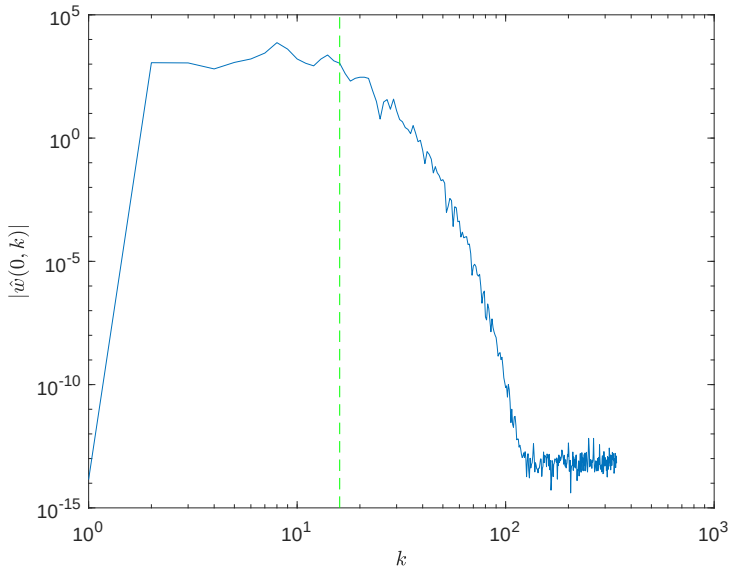

Figure 5.4: The spectrum in Fourier space of the initial condition $w_0(x)$, with the vertical line (green, dashed) indicating the maximum resolved wavenumber k_{max}.

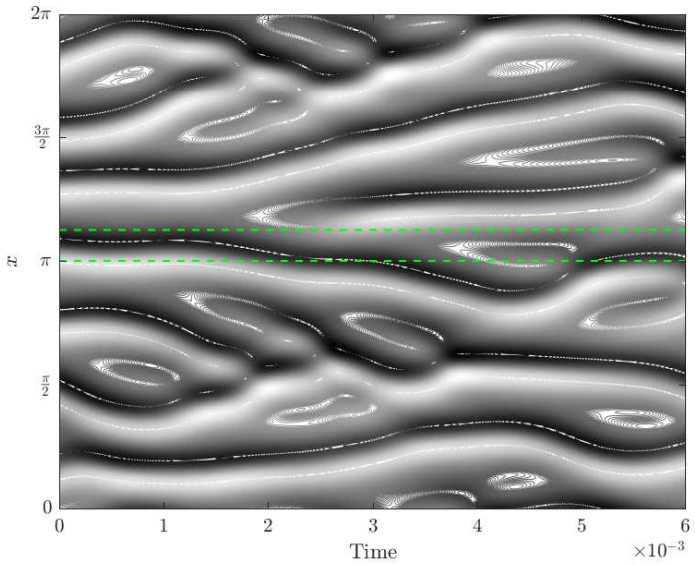

Figure 5.5: A space-time contour plot of the DNS solution, solved up to $t = 2T$. The horizontal lines (green, dashed) indicate the length scale corresponding to the maximum resolved wavenumber $k_{max} = 16$.

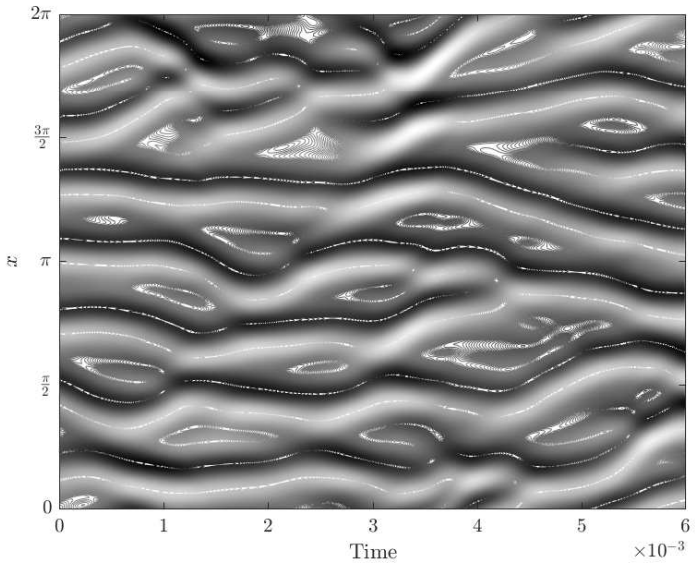

Figure 5.6: A space-time contour plot of the LES with no closure term solution, solved up to $t = 2T$.

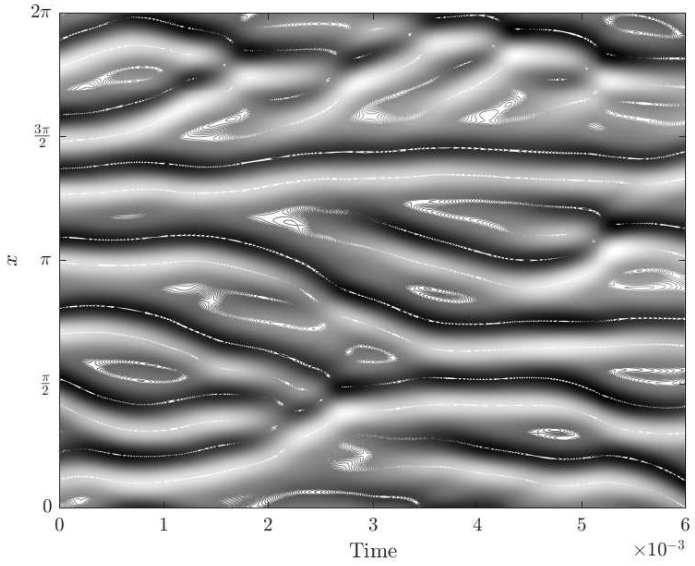

Figure 5.7: A space-time contour plot of the LES with the closure given in terms initial guess ν_0 solution, solved up to $t = 2T$.

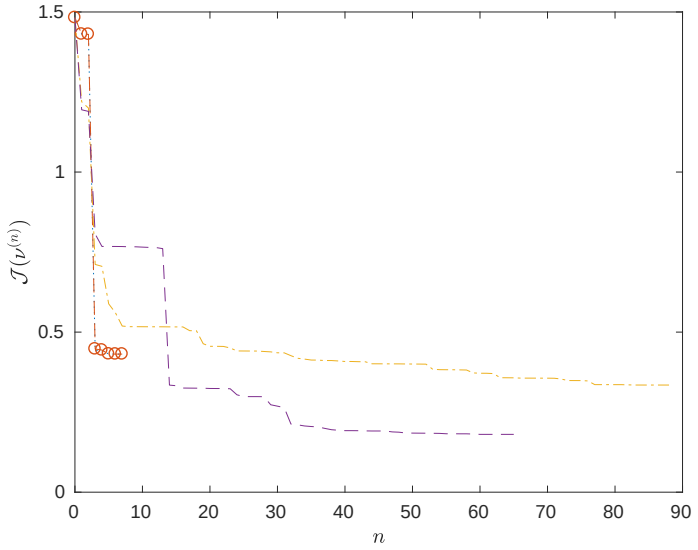

Figure 5.8: The decrease of the cost functional $\mathcal{J}(\nu^{(n)})$, given in (2.12), as function of iteration n for Sobolev parameters given in Table 5.1: Case A (blue, dots), Case B (red, circles), Case C (yellow, dash-dot), and Case D (purple, dashed).

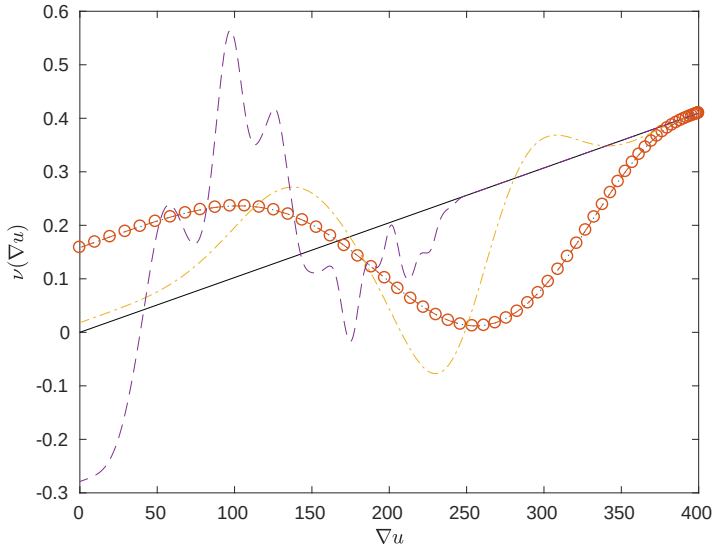

Figure 5.9: The optimal eddy viscosity $\check{\nu}$ for Sobolev parameters given in Table 5.1: Case A (blue, dots), Case B (red, circles), Case C (yellow, dash-dot), and Case D (purple, dashed). The optimal eddy viscosity is compared to the initial guess given in (3.3) (black, solid line).

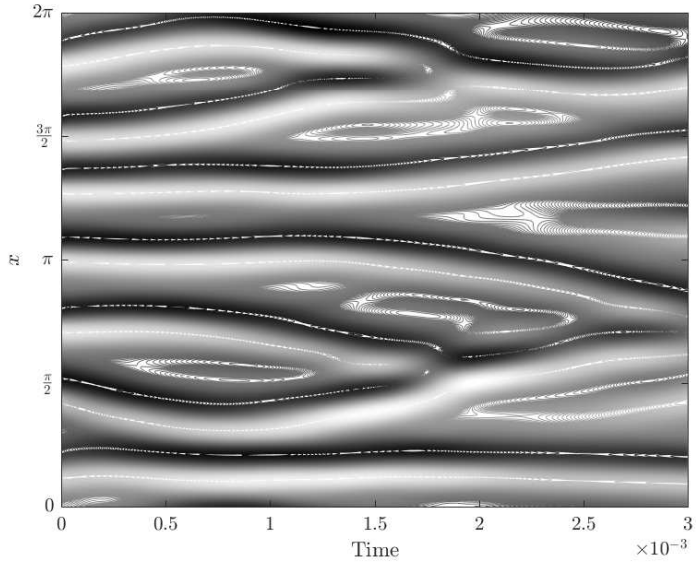

(a)

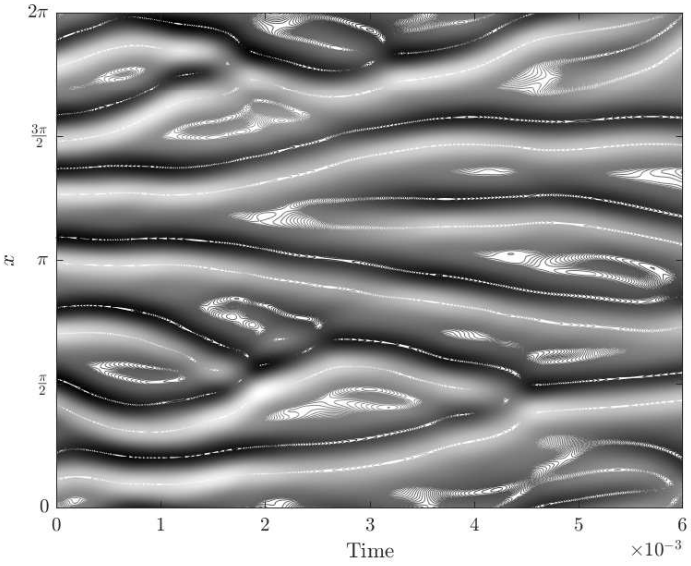

(b)

Figure 5.10: Space-time contour plots for LES with optimal eddy viscosity $\check{\nu}$ from: (a) Case C in Table 5.1, and (b) Case D in Table 5.1, solved up to $t = 2T$.

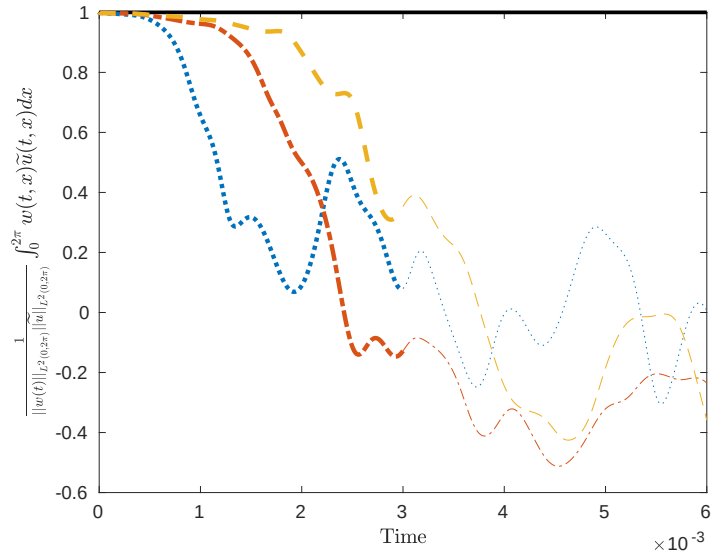

(a)

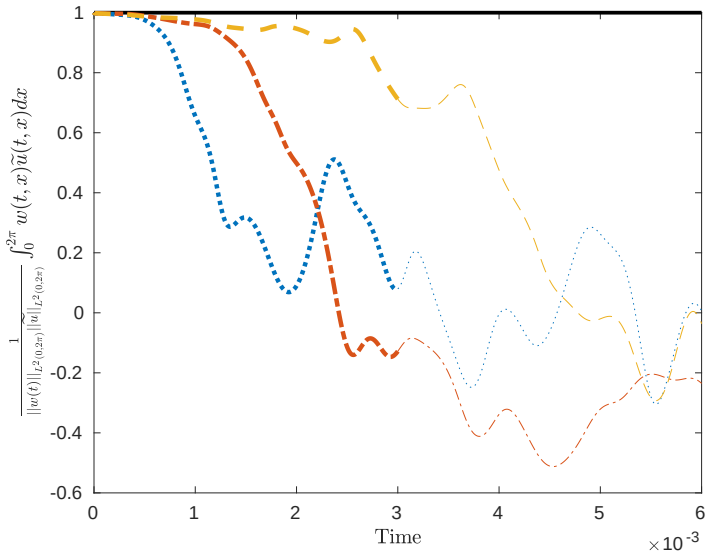

(b)

Figure 5.11: The first diagnostic quantity $E_1(t)$ given in (5.1), for the optimal eddy viscosity $\check{\nu}$ from: (a) Case C in Table 5.1, and (b) Case D in Table 5.1. Shown is when $\widetilde{u}(t,x)$ is set as: DNS (black, solid line), LES with no closure term (blue, dots), LES with the closure given in terms initial guess ν_0 (red, dash-dot), and the LES with the optimal eddy viscosity $\check{\nu}$ (yellow, dashed). The optimal eddy viscosity is optimized for $t = [0, T]$ (bold lines), and here we show for up to $t = 2T$ (outside of the "training" interval are the thin plots).

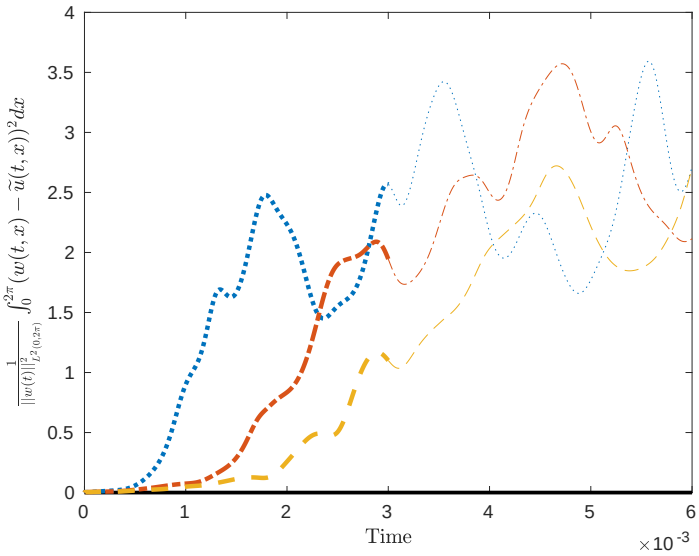

(a)

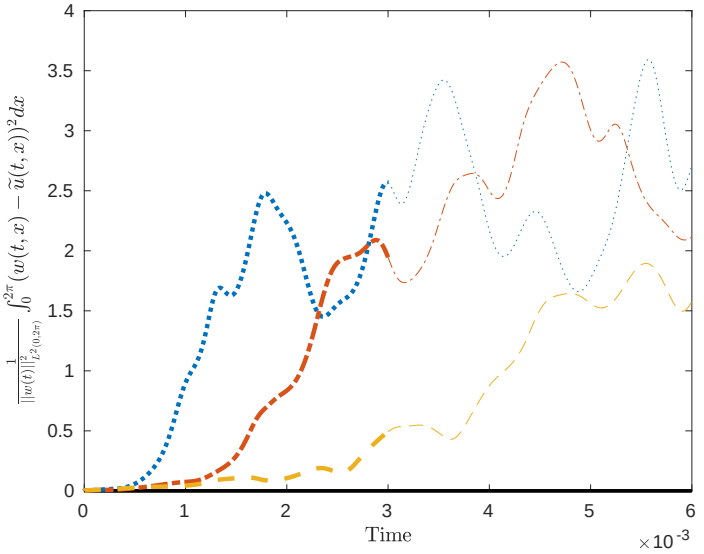

(b)

Figure 5.12: The second diagnostic quantity $E_2(t)$ given in (5.2), for the optimal eddy viscosity $\check{\nu}$ from: (a) Case C in Table 5.1, and (b) Case D in Table 5.1. Shown is when $\widetilde{u}(t,x)$ is set as: DNS (black, solid line), LES with no closure term (blue, dots), LES with the closure given in terms initial guess ν_0 (red, dash-dot), and the LES with the optimal eddy viscosity $\check{\nu}$ (yellow, dashed). The optimal eddy viscosity is optimized for $t = [0, T]$ (bold lines), and here we show for up to $t = 2T$ (outside of the "training" interval are the thin plots).

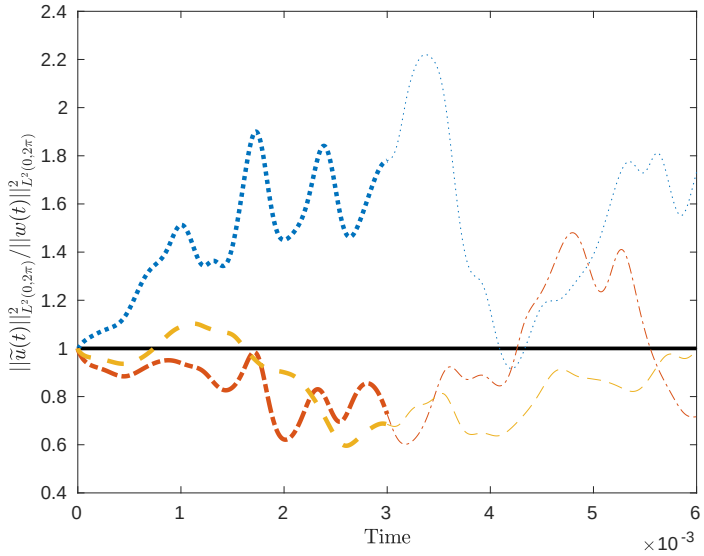

(a)

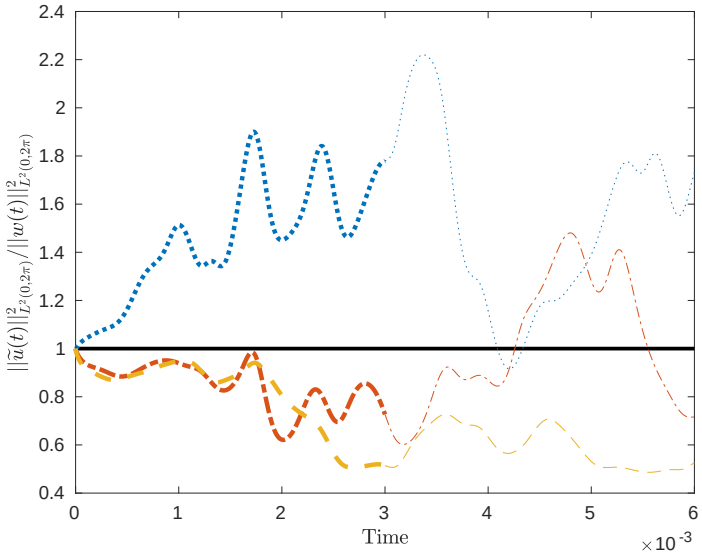

(b)

Figure 5.13: The normalized kinetic energy $K(t)$ given in (5.3), for the optimal eddy viscosity $\check{\nu}$ from: (a) Case C in Table 5.1, and (b) Case D in Table 5.1. Shown is when $\widetilde{u}(t,x)$ is set as: DNS (black, solid line), LES with no closure term (blue, dots), LES with the closure given in terms initial guess ν_0 (red, dash-dot), and the LES with the optimal eddy viscosity $\check{\nu}$ (yellow, dashed). The optimal eddy viscosity is optimized for $t = [0, T]$ (bold lines), and here we show for up to $t = 2T$ (outside of the "training" interval are the thin plots).

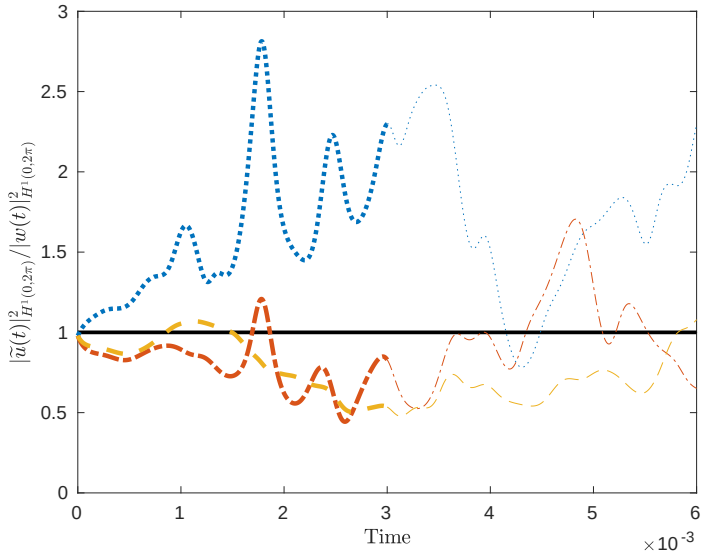

(a)

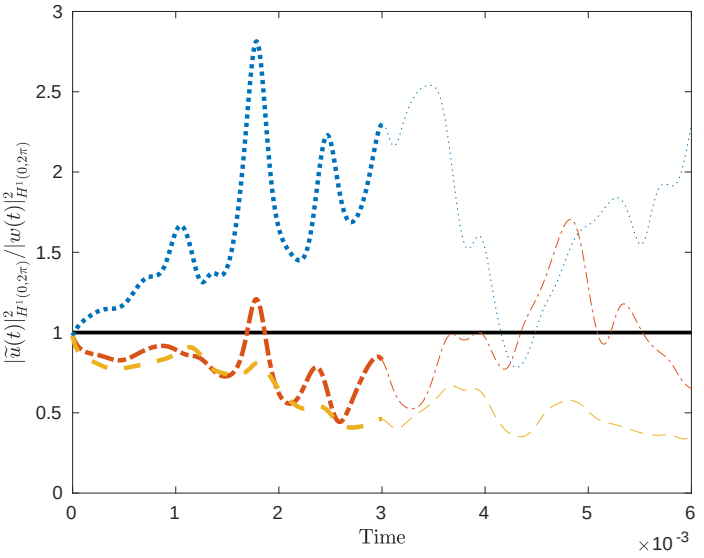

(b)

Figure 5.14: The normalized enstrophy $E_3(t)$ given in (5.4), for the optimal eddy viscosity $\check{\nu}$ from: (a) Case C in Table 5.1, and (b) Case D in Table 5.1. Shown is when $\widetilde{u}(t,x)$ is set as: DNS (black, solid line), LES with no closure term (blue, dots), LES with the closure given in terms initial guess ν_0 (red, dash-dot), and the LES with the optimal eddy viscosity $\check{\nu}$ (yellow, dashed). The optimal eddy viscosity is optimized for $t = [0, T]$ (bold lines), and here we show for up to $t = 2T$ (outside of the "training" interval are the thin plots).

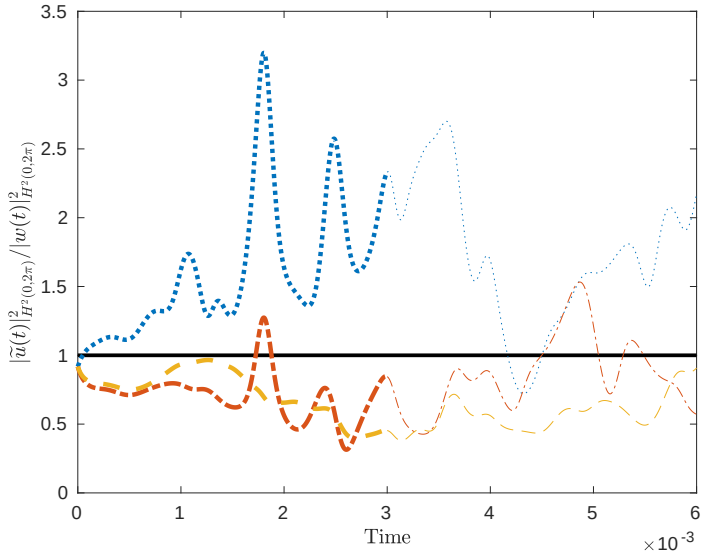

(a)

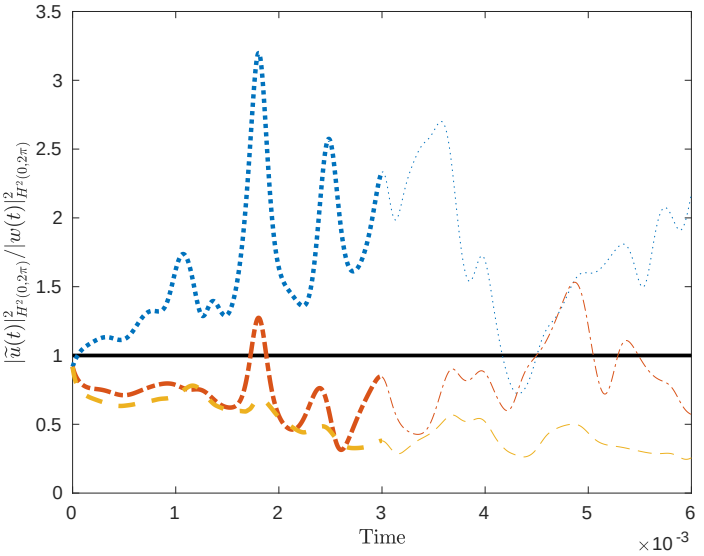

(b)

Figure 5.15: The normalized H^2 seminorm $E_4(t)$ given in (5.5), for the optimal eddy viscosity $\check{\nu}$ from: (a) Case C in Table 5.1, and (b) Case D in Table 5.1. Shown is when $\widetilde{u}(t,x)$ is set as: DNS (black, solid line), LES with no closure term (blue, dots), LES with the closure given in terms initial guess ν_0 (red, dash-dot), and the LES with the optimal eddy viscosity $\check{\nu}$ (yellow, dashed). The optimal eddy viscosity is optimized for $t = [0, T]$ (bold lines), and here we show for up to $t = 2T$ (outside of the "training" interval are the thin plots).

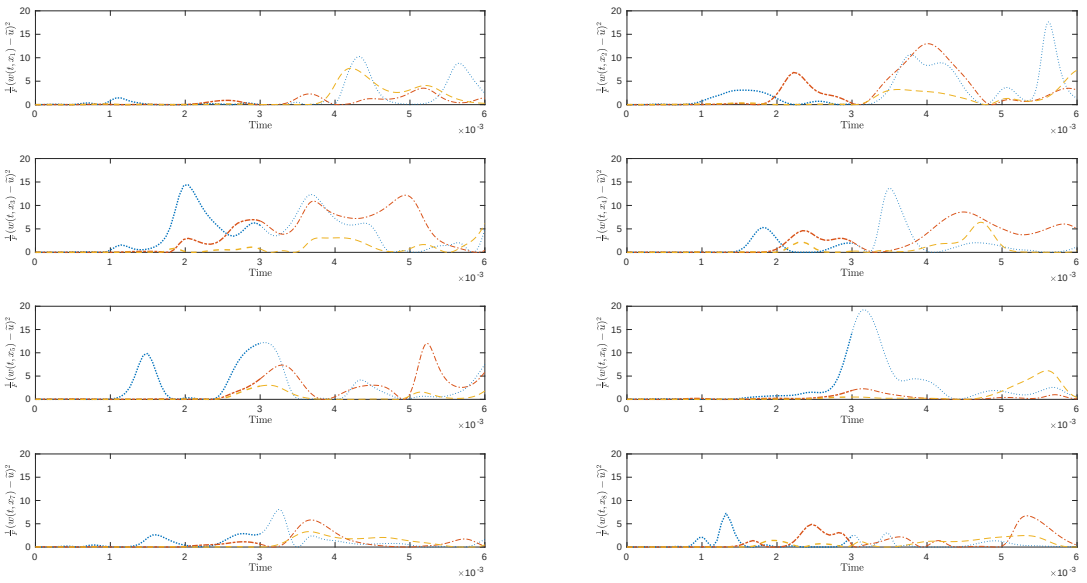

Figure 5.16: The error at each observation point x_i ($i = 1, \ldots, 8$ shown from left to right, top to bottom), for the optimal eddy viscosity $\check{\nu}$ from Case C in Table 5.1. Shown is when $\widetilde{u}(t, x)$ is set as: LES with no closure term (blue, dots), LES with the closure given in terms initial guess ν_0 (red, dash-dot), and the LES with the optimal eddy viscosity $\check{\nu}$ (yellow, dashed). The optimal eddy viscosity is optimized for $t = [0, T]$ (bold lines), and here we show for up to $t = 2T$ (outside of the "training" interval are the thin plots).

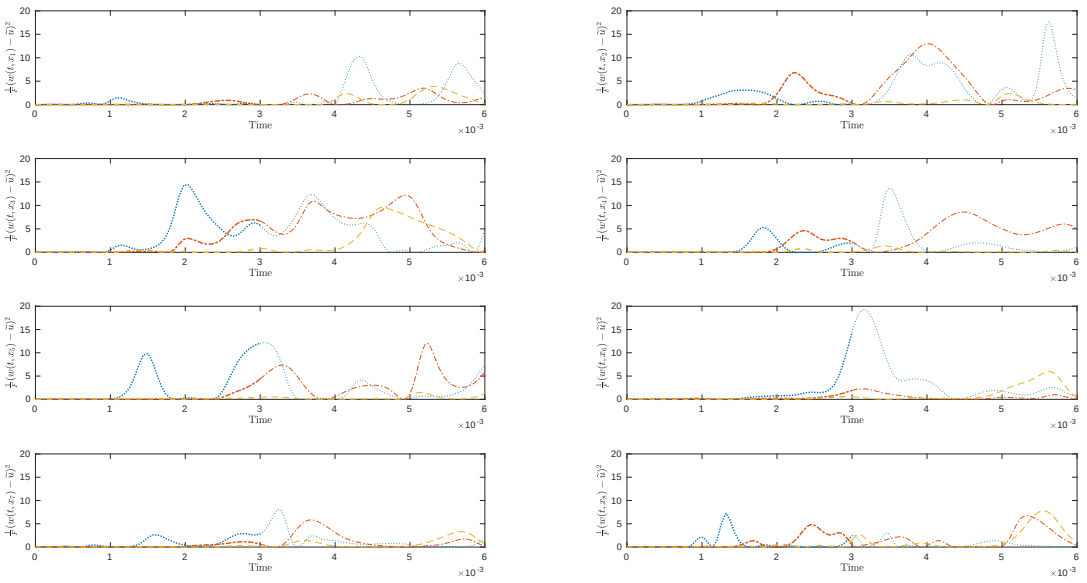

Figure 5.17: The error at each observation point x_i ($i = 1, \ldots, 8$ shown from left to right, top to bottom), for the optimal eddy viscosity $\check{\nu}$ from Case D in Table 5.1. Shown is when $\widetilde{u}(t, x)$ is set as: LES with no closure term (blue, dots), LES with the closure given in terms initial guess ν_0 (red, dash-dot), and the LES with the optimal eddy viscosity $\check{\nu}$ (yellow, dashed). The optimal eddy viscosity is optimized for $t = [0, T]$ (bold lines), and here we show for up to $t = 2T$ (outside of the "training" interval are the thin plots).

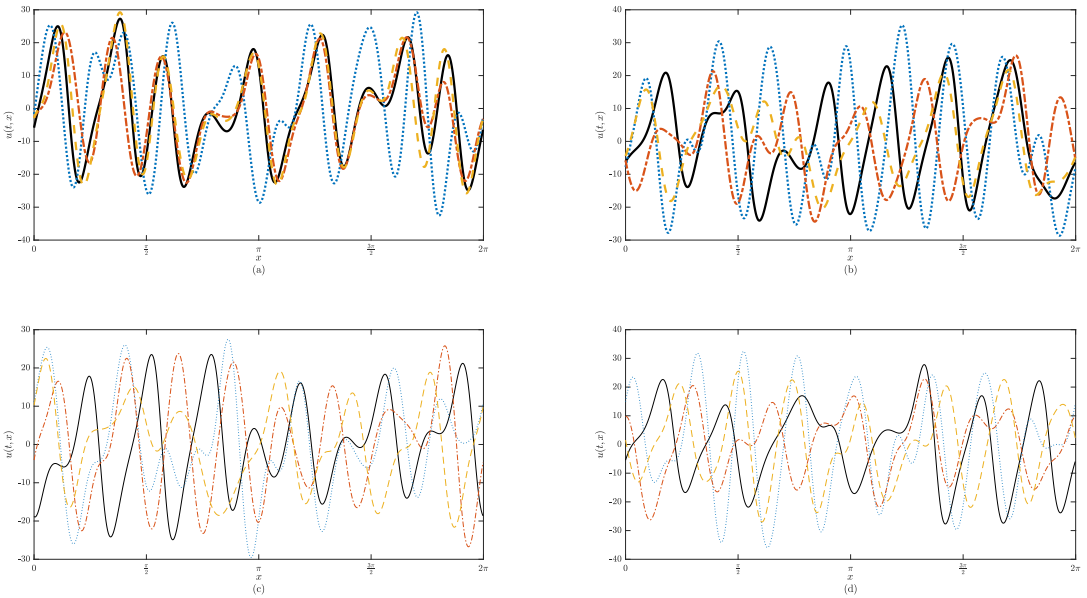

Figure 5.18: Plot of the solutions in physical space, for the optimal eddy viscosity $\check{\nu}$ from Case C in Table 5.1, at particular points in time: (a) $t = 15 \times 10^{-4}$, (b) $t = 30 \times 10^{-4}$, (c) $t = 45 \times 10^{-4}$, and (d) $t = 60 \times 10^{-4}$. Shown is when $\widetilde{u}(t, x)$ is set as: DNS (black, solid line), LES with no closure term (blue, dots), LES with the closure given in terms initial guess ν_0 (red, dash-dot), and the LES with the optimal eddy viscosity $\check{\nu}$ (yellow, dashed). The optimal eddy viscosity is optimized for $t = [0, T]$ (bold lines, (a) and (b)), and here we show for up to $t = 2T$ (outside of the "training" interval are the thin plots, (c) and (d)).

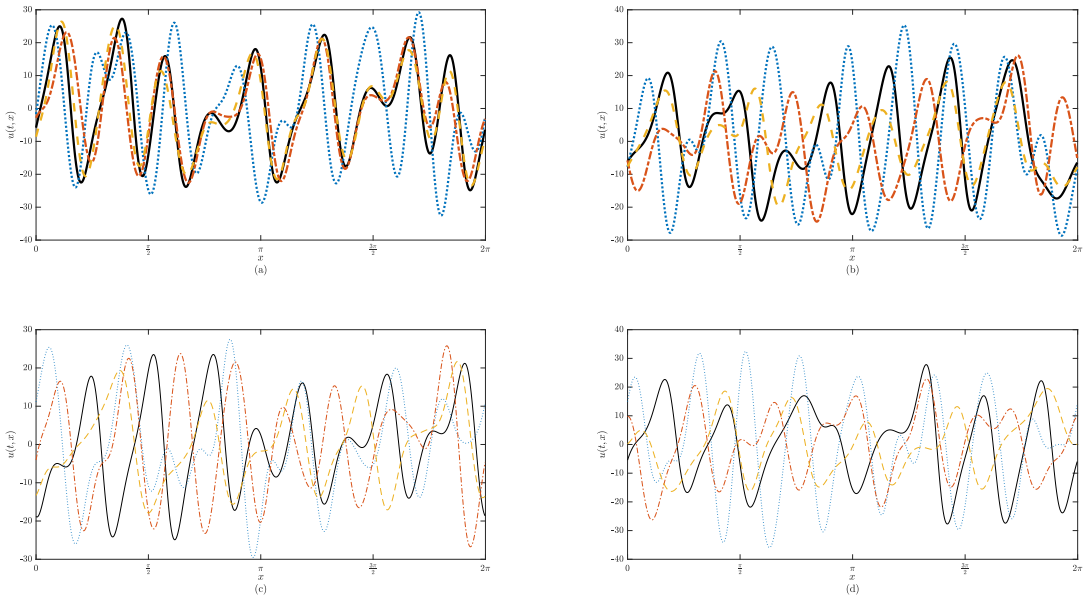

Figure 5.19: Plot of the solutions in physical space, for the optimal eddy viscosity $\check{\nu}$ from Case D in Table 5.1, at particular points in time: (a) $t = 15 \times 10^{-4}$, (b) $t = 30 \times 10^{-4}$, (c) $t = 45 \times 10^{-4}$, and (d) $t = 60 \times 10^{-4}$. Shown is when $\widetilde{u}(t, x)$ is set as: DNS (black, solid line), LES with no closure term (blue, dots), LES with the closure given in terms initial guess ν_0 (red, dash-dot), and the LES with the optimal eddy viscosity $\check{\nu}$ (yellow, dashed). The optimal eddy viscosity is optimized for $t = [0, T]$ (bold lines, (a) and (b)), and here we show for up to $t = 2T$ (outside of the "training" interval are the thin plots, (c) and (d)).

Chapter 6

Discussion

In this investigation, we determined an optimal eddy viscosity closure in the general form as the Smagorinsky model. From the results shown in Chapter 5, we were able to construct various eddy viscosities that locally minimize the cost functional, by simply modifying the Sobolev length scale parameters to control the smoothness of the eddy viscosity. In particular, we explored two good sets of Sobolev parameters denoted Case C and Case D in Table 5.1. As shown in Figure 5.9, we can see that Case C produces a smooth eddy viscosity, where as Case D produces a less smooth eddy viscosity. So, we shall denote these as the "smooth" eddy viscosity and the "rough" eddy viscosity, respectively. From the values of the cost functional, shown in Figure 5.8, the rough eddy viscosity minimizes the cost functional better than the other eddy viscosities. Observing the intrinsic dynamics of the LES solutions using the smooth eddy viscosity and the rough eddy viscosity, shown in Figures 5.10(a) and 5.10(b) respectively, we can see the two solution fields contain different dynamics.

In the space-time contour plot in Figure 5.10(b), we can see the solution contours merging and separating. We also see these interactions in the DNS contour plot given in Figure 5.5. These characteristic "events" occur beyond the "training" window, and the rough eddy viscosity attempts to encompass these characteristics.

Considering the first diagnostics quantity (5.1) to be a cosine of the "angle", we can see in Figure 5.11(a) and 5.11(b) that the DNS, our "exact" solution, is equal to 1 for all time as should be expected. In both Figure 5.11(a) and 5.11(b), the optimal eddy viscosities perform better than the LES with no closure and the LES with the closure given in terms initial guess ν_0. It should be noted that once the value of (5.1) drops to 0, this signals that the functions w and $\widetilde{u}$ have become orthogonal. Figure 5.11(a) shows that the smooth eddy viscosity attains orthogonality shortly after the "training" window. Where-as, the rough eddy viscosity does not become orthogonal for a longer interval.

The second diagnostics quantity (5.2) in Figure 5.12(a) and 5.12(b), also shows that the LES solutions obtained with the optimal eddy viscosities are closer to the DNS compared to the LES with no closure and the LES with the closure given in terms initial guess ν_0. However, looking at the kinetic energy (5.3), enstrophy (5.4), and H^2 seminorm (5.5) (Figure 5.13(a), 5.14(a), and 5.15(a) respectively for the smooth eddy viscosity and Figure 5.13(b), 5.14(b), and 5.15(b) respectively for the rough eddy viscosity) the figures show that the energy in the system is comparable to the Smagorinsky initial guess ν_0. Due to the lack of sufficient dissipation in the system, it is shown that LES with no closure term in general has more energy than the DNS. Both LES with closure terms predominantly have less energy in the system than the

DNS. This indicates that the closure terms may be too dissipative. We shall also note that both the smooth and the rough eddy viscosity in Figure 5.9 occasionally attains negative values, which implies that they are not strictly dissipative but also add energy into the system for certain values of $\left(\frac{\partial \widetilde{u}}{\partial x}\right)^2$. In addition, the optimal eddy viscosities typically do not equal zero when velocity gradients equal zero but it does vanish for certain other values.

In Figures 5.16 and 5.17, the error (5.13) at the observation points (5.11) is much less that the LES with no closure and the initial guess ν_0. As well in Figures 5.18 and 5.19, we can see in the training interval the optimal eddy viscosities generally capture the behaviour of the DNS. Outside the training interval, as the solutions begin to diverge, the optimal eddy viscosity still able to produce the general behaviour of the DNS.

Chapter 7

Conclusion

In this study, we developed a mathematically rigorous approach for computationally constructing an optimal eddy viscosity closure based on the Smagorinsky model, for LES. To determine this optimal eddy viscosity, a PDE-constraint optimization problem and the use of a adjoint-based method was used to formulate a gradient of the state-dependent eddy viscosity. The optimal functional form of the eddy viscosity was determined in a very general (continuous) setting, then numerically solved, hence we used an "optimize then discretize" approach to determine the eddy viscosity. We also showed that a certain amount of regularity was required for the eddy viscosity, so a suitably smooth gradient was solved by using Sobolev gradients rather than a traditional L^2 gradient.

Multiple optimal eddy viscosities were obtained, varying due to the smoothing parameters applied to the Sobolev gradient. A smooth optimal eddy viscosity was found, which had significantly reduced the value of the cost functional. A smaller

value of the cost functional was obtained when using a less smooth eddy viscosity. This rough eddy viscosity was shown to better encompass the intrinsic behaviour of the flow field. It was shown that the optimal eddy viscosities out-performed the original Smagorinsky type initial guess for the eddy viscosity.

Future work that will be explored is to use this method for longer time intervals, as in this investigation we were limited to a short time interval due to the rapid divergence of the solutions. We are also interested investigating different observation operators, in particular observing points in Fourier space rather than in physical space. Incorporating more powerful tools used in calculus of variations, in order to improve our local optimizer will be something that will explored as well. Naturally, we also wish to extend this work to Navier-Stokes, which acted as the main motivation for this project. A similar approach will be attempted, using a Smagorinsky model with a state dependent eddy viscosity.

Bibliography

[1] J. P. Boyd. *Chebyshev and Fourier Spectral Methods*. Dover Publications, 2001.

[2] V. Bukshtynov and B. Protas. Optimal reconstruction of material properties in complex multiphysics phenomena. *Journal of Computational Physics*, 242:889–914, 2013.

[3] V. Bukshtynov, O. Volkov, and B. Protas. On optimal reconstruction of constitutive relations. *Physica D: Nonlinear Phenomena*, 240(16):1228–1244, 2011.

[4] J. M. Burgers. Application of a model system to illustrate some points of the statistical theory of free turbulence. In *Acad. Sci. Amsterdam*, volume 43, pages 2–12, 1940.

[5] J. D. Cole. On a quasi-linear parabolic equation occurring in aerodynamics. *Quarterly of applied mathematics*, 9(3):225–236, 1951.

[6] S. M. Cox and P. C. Matthews. Exponential Time Differencing for Stiff Systems. *Journal of Computational Physics*, 176(2):430–455, 2002.

[7] O. Darrigol. *Worlds of Flow: A History of Hydrodynamics from the Bernoullis to Prandtl*. Oxford University Press, 2005.

[8] A. Das and R. D. Moser. Optimal large-eddy simulation of forced Burgers equation. *Physics of Fluids*, 14(12):4344–4351, 2002.

[9] P. A. Davidson. *Turbulence: An Introduction for Scientists and Engineers*. Oxford University Press, USA, 2015.

[10] T. A. Driscoll, N. Hale, and L. N. Trefethen. *Chebfun Guide*. Pafnuty Publications, 2014.

[11] C. L. Fefferman. Existence and smoothness of the Navier-Stokes equation. *The millennium prize problems*, 57:67, 2006.

[12] U. Frisch. *Turbulence*. Cambridge University Press, 1995.

[13] E. Hopf. The partial differential equation $u_t + uu_x = \mu_{xx}$. *Communications on Pure and Applied mathematics*, 3(3):201–230, 1950.

[14] A. Kassam and L. N. Trefethen. Fourth-Order Time-Stepping for Stiff PDEs. *SIAM J. Scientific Computing*, 26(4):1214–1233, 2005.

[15] Y. Kuramoto. Diffusion-induced chaos in reaction systems. *Progress of Theoretical Physics Supplement*, 64:346–367, 1978.

[16] D. K. Lilly. A proposed modification of the Germano subgrid-scale closure method. *Physics of Fluids A: Fluid Dynamics*, 4(3):633–635, 1992.

[17] R. Maulik and O. San. Evaluation of explicit and implicit LES closures for Burgers turbulence. *arXiv preprint arXiv:1604.08649*, 2016.

[18] S. B. Pope. *Turbulent flows*. Cambridge University Press, 2000.

[19] W. H. Press. *Numerical recipes 3rd edition: The Art of Scientific Computing*. Cambridge University Press, 2007.

[20] T. C. Rebollo, E. D. Ávila, M. G. Mármol, F. Ballarin, and G. Rozza. On a certified Smagorinsky reduced basis turbulence model. *SIAM Journal on Numerical Analysis*, 55(6):3047–3067, 2017.

[21] W. Rodi, G. Constantinescu, and T. Stoesser. *Large-Eddy Simulation in Hydraulics*. Crc Press, 2013.

[22] G.I. Sivashinsky. Nonlinear analysis of hydrodynamic instability in laminar flames–I. Derivation of basic equations. In *Dynamics of Curved Fronts*, pages 459–488. Elsevier, 1988.

[23] J. Smagorinsky. General circulation experiments with the primitive equations: I. The basic experiment. *Monthly weather review*, 91(3):99–164, 1963.

[24] E. Tadmor. The well-posedness of the Kuramoto–Sivashinsky equation. *SIAM Journal on Mathematical analysis*, 17(4):884–893, 1986.

[25] H. Tennekes and J. L. Lumley. *A First Course in Turbulence*. MIT press, 1972.

[26] L. N. Trefethen. *Spectral Methods in MATLAB*. Society for Industrial and Applied Mathematics, Philadelphia, PA, USA, 2000.

[27] L. N. Trefethen. *Approximation Theory and Approximation Practice*. Philadelphia, PA: Society for Industrial and Applied Mathematics (SIAM), 2013.